Chemical Science



EDGE ARTICLE

View Article Online
View Journal | View Issue



Cite this: Chem. Sci., 2024, 15, 11321

All publication charges for this article have been paid for by the Royal Society of Chemistry

Coordination of Al(C_6F_5)₃ vs. B(C_6F_5)₃ on group 6 end-on dinitrogen complexes: chemical and structural divergences†

The coordination of the Lewis superacid tris(pentafluorophenyl)alane (AICF) to phosphine-supported, group 6 bis(dinitrogen) complexes $[ML_2(N_2)_2]$ is explored, with M = Cr, Mo or W and L = dppe (1,2bis(diphenylphosphino)ethane), depe (1,2-bis(diethylphosphino)ethane), dmpe (1,2-bis(dimethylphosphino) ethane) or 2 × PMe₂Ph. Akin to tris(pentafluorophenyl)borane (BCF), AlCF can form 1:1 adducts by coordination to one distal nitrogen of general formula $trans-[ML_2(N_2)\{(\mu-\eta^1:\eta^1-N_2)Al(C_6F_5)_3\}]$. The boron and aluminium adducts are structurally similar, showing a comparable level of N₂ push-pull activation. A notable exception is a bent (BCF adducts) vs. linear (AlCF adducts) M-N-N-LA motif (LA = Lewis acid), explained computationally as the result of steric repulsion. A striking difference arose when the formation of two-fold adducts was conducted. While in the case of BCF the 2:1 Lewis pairs could be observed in equilibrium with the 1:1 adduct and free borane but resisted isolation, AICF forms robust 2:1 adducts $trans-[ML_2\{(\mu-\eta^1:\eta^1-N_2)Al(C_6F_5)_3\}_2]$ that isomerise into a more stable *cis* configuration. These compounds could be isolated and structurally characterized, and represent the first examples of trinuclear heterometallic complexes formed by Lewis acid-base interaction exhibiting p and d elements. Calculations also demonstrate that from the bare complex to the two-fold aluminium adduct, substantial decrease of the HOMO-LUMO gap is observed, and, unlike the trans adducts (1:1 and 1:2) for which the HOMO was computed to be a pure d orbital, the one of the cis-trinuclear compounds mixes a d orbital with a π^* one of each N_2 ligands. This may translate into a more favourable electrophilic attack on the N_2 ligands instead of the metal centre, while a stabilized N2-centered LUMO should ease electron transfer, suggesting Lewis acids could be co-activators for electro-catalysed N2 reduction. Experimental UV-vis spectra for the tungsten family of compounds were compared with TD-DFT calculations (CAM-B3LYP/ def2-TZVP), allowing to assign the low extinction bands found in the visible spectrum to unusual lowlying MLCT involving N2-centered orbitals. As significant red-shifts are observed upon LA coordination, this could have important implications for the development of visible light-driven nitrogen fixation.

Received 24th April 2024 Accepted 14th June 2024

DOI: 10.1039/d4sc02713b

rsc.li/chemical-science

Introduction

Since the discovery of the first transition metal (TM) dinitrogen complex in 1965,¹ the quest for an efficient and mild process for dinitrogen transformation embodies an ultimate goal for chemists. Although much progress has been made in the last two decades in the field of artificial nitrogen fixation, the number of catalytic systems for N₂ conversion under

homogeneous conditions remains limited. 2,3 Therefore, new molecular design strategies must be explored to overcome the current scientific barriers and to gain access to optimised N_2 conversion.

Donor–acceptor activation is a strategy that has not been largely implemented in N₂ chemistry involving molecular complexes. This parallels neither its success for other small molecules activation, *e.g.*, CO₂ ⁴⁻⁶ or H₂,⁷⁻⁹ both well exemplified through frustrated Lewis pair (FLP) chemistry^{10–17} and metalligand cooperativity, ^{18,19} nor the fact that this concept finds echo in the two main processes responsible for nitrogen fixation. With regard to the nitrogenase enzymes, the "push–pull hypothesis" surmises that the acidic residues found in the active site build H-bonds with the distal N of N₂ bound to the FeMo-cofactor, ^{20–24} thus increasing polarization of the diatomic molecule and facilitating its protonation. ^{25,26} Besides, promotion of the Haber–Bosch catalysts with electropositive elements

^aLCC-CNRS, Université de Toulouse, CNRS, UPS 205 Route de Narbonne, BP44099, F-31077 Toulouse Cedex 4, France. E-mail: antoine.simonneau@lcc-toulouse.fr ^bDepartment of Chemistry, Quantum Chemistry, TU Darmstadt, Peter-Grünberg-Str. 4, 6, 4287 Darmstadt, Germany

[†] Electronic supplementary information (ESI) available: General methods, experimental procedures, NMR spectra, crystallographic and computational details and CIF files. CCDC 2346952–2346961. For ESI and crystallographic data in CIF or other electronic format see DOI: https://doi.org/10.1039/d4sc02713b

lowers the barrier for N_2 dissociation due to electrostatic effects, which can be seen as another manifestation of N_2 donoracceptor activation.²⁷⁻³⁰

At the molecular level, it can be achieved by the Lewis acidbase pairing of terminal N2 complexes with Lewis acids, 31-33 which results in increased N2 polarisation due to enhanced back-bonding from the donor metal. This was pioneered by the Chatt group³⁴⁻³⁶ with neutral main-group Lewis acids, and was later further exemplified by the Fryzuk,37 Tuczek,38 Szymczak25 and Simonneau^{39,40} groups. Main group^{41,42} and transition metal cations⁴³ have also been shown to participate in such type of donor-acceptor systems. The "donor" partner is generally an early-to-mid transition metal with a low formal oxidation state, although a model of purely main-group N2 donor-acceptor activation system was proposed by the Stephan group.44 By providing an access to a highly polarised N2 unit, opportunities for the discovery of new reactivity patterns for dinitrogen complexes can arise, for instance N₂ protonation, ²⁵ silylation or borylation.39 In this context, the team of Szymczak and ours have focused on the coordination of the strong boron Lewis acid tris(pentafluorophenyl)borane, B(C₆F₅)₃ (BCF) with a series of group 6 and 8 (M = Mo, W, and Fe) phosphine N₂-complexes and have studied with DFT the implications for the N2 ligand. 25,39,43 We have recently shown in a computational study that binding LAs to transition-metal N2-complexes may shift their molecular orbital ordering.45 Thus, by levelling basicity and redox potentials, Lewis acid coordination to the N2 ligand may be an interesting way to mitigate overpotentials in homogeneous ammonia synthesis (electro)catalysed with metal complexes. Recently, we turned our interest towards Lewis Super Acids (LSA),46 driven by the curiosity of gauging the pushpull effect when the acceptor is an extremely electron-deficient species. We have shown that a two-channel activation by the means of a strongly electrophilic bis(borane) C₆F₄{B(C₆F₅)₂}₂ (B₂CF) imparts significant activation to the diatomic molecule, up to the diazene-diide (N₂²⁻) state. 40 In the continuation of this work, we decided to study the coordination of the aluminium analogue of BCF, tris(pentafluorophenyl)alane - Al(C₆F₅)₃ (AICF)⁴⁷⁻⁵⁶ - to group 6 dinitrogen complexes, in order to assess how the resulting Lewis pairs differ or not in terms of structure and reactivity with respect to BCF.

AICF is structurally close to BCF as they both feature three C₆F₅ ligands in their coordination sphere and a central trivalent group 13 element, differing by their metal radii and electronegativity.57 This apparently anecdotic distinction turns out to change quite significantly their chemical properties. As a matter of fact, while BCF is notably stable in a trigonal planar geometry and do not interact with weak and even moderate donors (such as non-polar and aromatic molecules and even oxygen-based compounds),58,59 AICF is highly reactive (thermal and shock sensitive) in this configuration and is only stable in a tetrahedral environment where the 4th position is occupied by a weak donor^{49,51,53,60} or, in its unsolvated dimeric form, through double Al-F interactions between Al and the ortho-F atom of one C₆F₅ ring.53 This singular aspect to form adducts with very weak donors (vide infra) suggests indeed higher electrophilic properties of AICF vs. BCF, and it is now widely accepted that AICF has

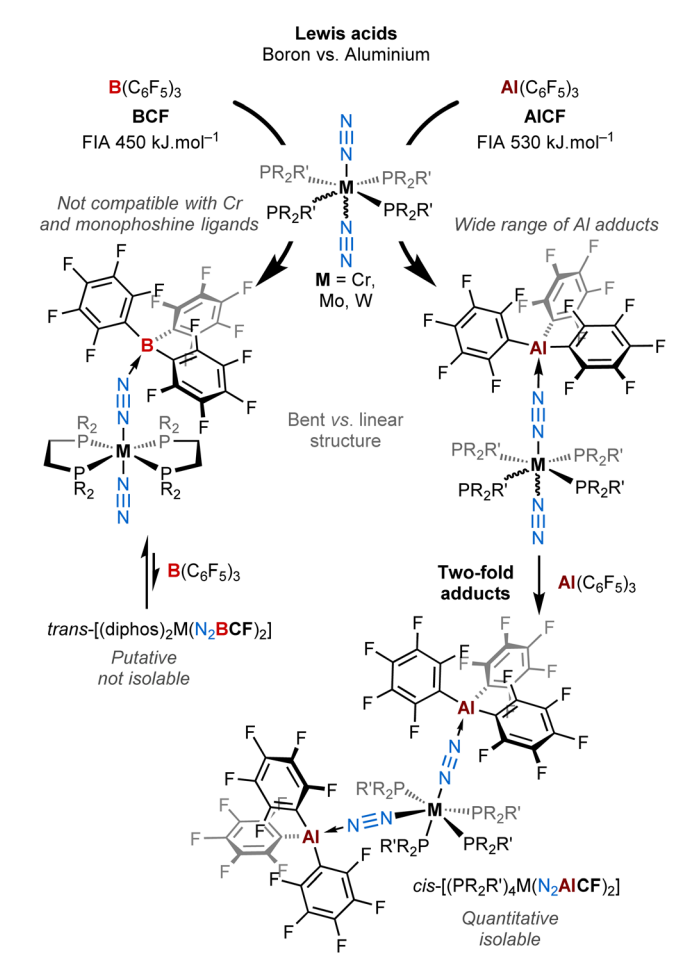


Fig. 1 Coordination of AICF versus BCF on Group 6 end-on dinitrogen complexes leading to a new family of mono and double Al dinitrogen adducts.

a much stronger Lewis acid character than BCF.⁵⁶ From computational studies and compiled experimental data, AlCF is considered as an LSA, having a Fluoride Ion Affinity (FIA)⁶¹ – acknowledged to be a way to estimate Lewis acidity – of 530 kJ mol⁻¹. In ascending order, the latter has an FIA higher than B_2CF (523 kJ mol⁻¹), SbF₅ (490 kJ mol⁻¹) (the reference of the LSA scale), and much higher than BCF (450 kJ mol⁻¹).^{53,56,62-65}

In this work, we describe a new family of **AICF** adducts with Chatt-Hidai type group 6 dinitrogen complexes, by the means of spectroscopy (NMR, IR, UV-vis), single crystal X-ray diffraction (sc-XRD), and DFT calculations. Notable chemical and structural discrepancies are observed by comparison to **BCF** (see Fig. 1), which are duly highlighted throughout the article. Remarkably, the switch from boron to aluminium allowed us to isolate bis(μ - η^1 : η^1 - N_2 -**AICF**) adducts that remained elusive in the case of **BCF**. These are the first examples of neutral two-fold adducts of a main group Lewis acid with a bis(dinitrogen) complex.

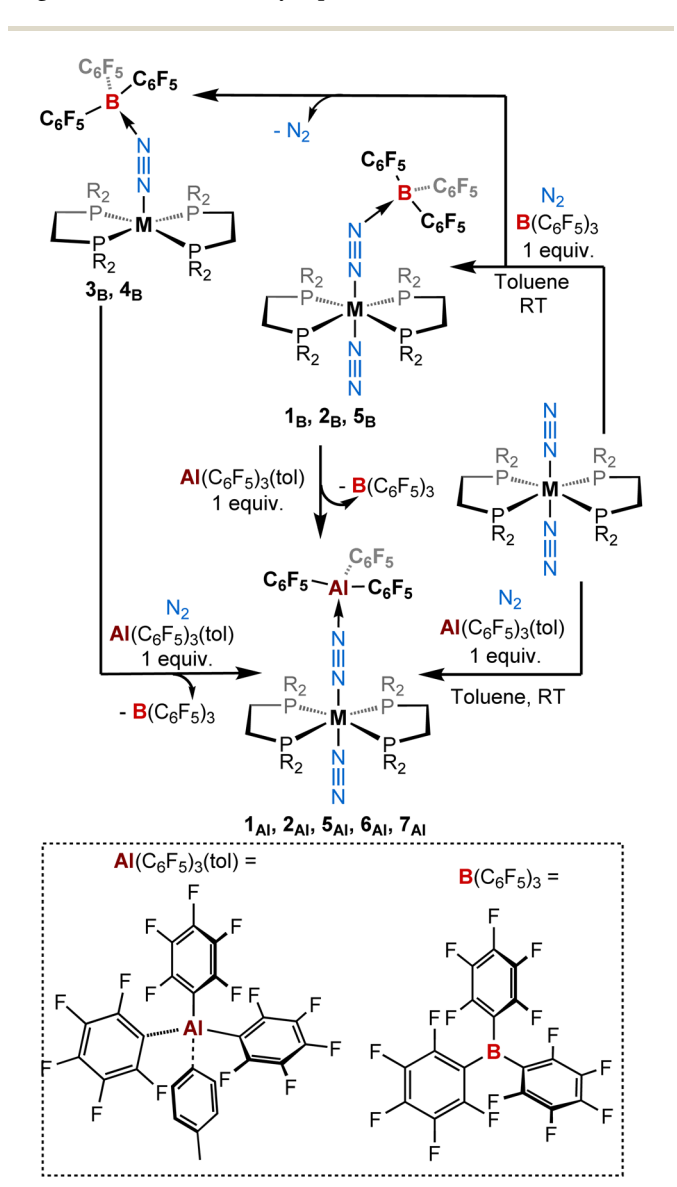
Results and discussion

Syntheses of 1:1 adducts supported with bis(phosphines)

Stoichiometric treatment (1:1) of tris(pentafluorophenyl)alane toluene adduct⁵¹ with a series of dinitrogen complexes *trans*-

Edge Article Chemical Science

 $[ML_2(N_2)_2]$ in toluene (M = W, Mo, and Cr; L = 1,2-bis(diethylphosphino)ethane [depe] or 1,2-bis(diphenylphosphino)ethane [dppe] or 1,2-bis(dimethylphosphino)ethane [dmpe])43,66-75 under a dinitrogen atmosphere produced new 1:1 adducts $[ML_2(N_2)(\mu-N_2)Al(C_6F_5)_3]$ $\mathbf{1_{Al}}$, $\mathbf{2_{Al}}$, $\mathbf{5_{Al}}$, $\mathbf{6_{Al}}$, and $\mathbf{7_{Al}}$ of trans configuration in moderate to excellent yields (Scheme 1 and Table 1). Note that better results in terms of analytical purity, yields, and reproducibility have been obtained with the depe and dmpe series (see ESI†). Adducts 1_{Al}, 2_{Al}, 5_{Al}, 6_{Al} and 7_{Al} were characterised in solution and in the solid-state by multi-nuclei NMR and IR spectroscopies as well as single-crystal XRD analysis. Similarities are found between the depe-supported complexes 1_{Al}, 2_{Al} and their boron analogues 1_B, 2_B. Indeed, NMR signatures of these species are very close especially when considering their ³¹P NMR resonance (see Table 3). Coordination of the LA (BCF or AlCF) at the distal nitrogen of the N2 fragment induces a nearly equal bathochromic shift of the µ-



Scheme 1 Reactivity of $ML_2(N_2)_2$ (M=W, Mo, Cr; L= depe, dppe, dmpe) complexes with (top) $B(C_6F_5)_3$ and (bottom) $Al(C_6F_5)_3$ (tol) (1 equiv.) under a dinitrogen atmosphere.

Table 1 Description of the different adducts

 a LA = Lewis acid. b NMR yield.

Compound	LA^a	M	R	Config.	N ₂ motifs	Yield (%)
1 _{AL}	AlCF	W	Et	trans	μ-N ₂ , η-N ₂	89
1 _B ⁴³	BCF	W	Et	trans	μ -N ₂ , η -N ₂	62
241	AlCF	Mo	Et	trans	μ -N ₂ , η -N ₂	100
$\mathbf{2_B}^{43}$	BCF	Mo	Et	trans	μ -N ₂ , η -N ₂	53
3 _B	BCF	W	Ph	trans	μ - N_2	${31}^{b}$
$4_{\rm B}$	BCF	Mo	Ph	trans	μ - N_2	${95}^{b}$
5_{AL}	AlCF	W	Ph	trans	μ - N_2 , η - N_2	51
5_{B}	BCF	W	Ph	trans	μ -N ₂ , η -N ₂	$\{69\}^{b}$
6_{AL}	AlCF	Mo	Ph	trans	μ - N_2 , η - N_2	81
7_{AL}	AlCF	Cr	Me	trans	μ - N_2 , η - N_2	79

 $N \equiv N$ IR band and hypsochromic shift of the terminal $N \equiv N$ stretching mode (see Table 3).

Suitable single-crystals of $\mathbf{1_{Al}}$ and $\mathbf{2_{Al}}$ for XRD studies have been grown from a cold and saturated solution of toluene/n-pentane. The solid-state structures of $\mathbf{1_{Al}}$ and $\mathbf{2_{Al}}$ (see Fig. 3, left, for $\mathbf{1_{Al}}$ and ESI† for $\mathbf{2_{Al}}$) depict a similar octahedral geometry around the group 6 metal to that of $\mathbf{1_{B}}$ and $\mathbf{2_{B}}$. Expectedly, coordination of AlCF to the distal N atom in complexes $\mathbf{1_{Al}}$ and $\mathbf{2_{Al}}$ imparts a tetrahedral geometry around the Al center (angles averaged at 109.5° for $\mathbf{1_{Al}}$ and 108.0° for $\mathbf{2_{Al}}$). The $\mathbf{N_{1}}$ – $\mathbf{N_{2}}$ bond lengths are similar between the aluminium and boron analogues (see Table 3). The TM- $\mathbf{N_{1}}$ distance is slightly shortened in the case of aluminium adducts (W- $\mathbf{N_{1}}$ = 1.855 Å for $\mathbf{1_{Al}}$ νs . 1.909 Å for $\mathbf{1_{B}}$ and Mo- $\mathbf{N_{1}}$ = 1.869 Å for $\mathbf{2_{Al}}$ νs . 1.894 Å for $\mathbf{2_{B}}$).

Overall, these experimental data point to a diminished bond order for the N₂ unit as a result of enhanced back-donation with a similar "push-pull" activation level of μ -N₂ in species 1_{Al} , 2_{Al} and $1_{\rm B}$, $2_{\rm B}$. However, we noticed structural divergences between 1_{Al}, 2_{Al} and their boron analogues 1_B, 2_B. According to the Cambridge Structural Database (CSD), the Al₁-N₂ bond lengths – 1.817 Å for $\mathbf{1}_{Al}$ and 1.842 Å for $\mathbf{2}_{Al}$ – are found to be the shortest ones compared to the expected Al-N distances range for similar reported N-Al(C_6F_5)₃ motifs (from 1.853 Å 76,77 to 2.167 Å 78) and N_2 -AlR₃ (R = alkyl) fragments (from 1.929 Å ⁷⁹ to 2.089 Å ⁸⁰). On the other hand, the B-N₂ length for the boron congeners (1.549 Å for $\mathbf{1}_{B}$ and 1.562 Å for $\mathbf{2}_{B}$) are found in the expected B-N distances range for similar reported N-B(C₆F₅)₃ moieties (from 1.492 Å 81 to 1.807 Å 82) but are slightly below the B-N distances range for comparable bridging diazo borane (μ-N₂)-B(C₆F₅)₃ and azido borane (μ -N₃)-B(C₆F₅)₃ fragments (from 1.575 Å ²⁵ to 1.678 Å 38). These results thus advocate for the presence of robust interactions between the bridging N₂ and the LA centre, more prominent in the case of aluminium.

Experimentally, we demonstrated the stronger affinity of μ -N₂ motif for **AlCF** ν s. **BCF** by treating adduct $\mathbf{1}_B$ with one equivalent of $Al(C_6F_5)_3(tol)$ that leads to the formation of $\mathbf{1}_{Al}$ and free **BCF** with an NMR yield higher than 90% (see Scheme 1 and ESI†). Note that over time this equilibrium does not evolve showing that the formation of $\mathbf{1}_{Al}$ from $\mathbf{1}_B$ is thermodynamically favourable. This set of clues led us to analyse the N₁-N₂-LA angle. In the case of the aluminium adducts, a nearly straight

 N_1-N_2-Al angle is found - 168.4° and 167.8° for $\mathbf{1}_{Al}$ and $\mathbf{2}_{Al}$, respectively. These data conflict with similar reported N=N-Al angles of bridging diazenido trialkylaluminum (μ-N=N)-AlR₃ and azido trialkylaluminum (μ-N=N)-AlR₃ species featuring values ranging from 105.5° 80 to 158.9°.84 These results also contrast with the bent N₁-N₂-B angle found for the boron analogues – 148.4° for $\mathbf{1}_{B}$ and 150.9° for $\mathbf{2}_{B}$. While $[M(depe)_2(N_2)_2]$ and $[M(dppe)_2(N_2)_2]$ cleanly reacted with BCF to form quantitatively 1:1 adducts, we observed significant divergent behaviours when we engaged trans-[Cr(dmpe)₂(N₂)₂] with BCF. Indeed, this leads to a partial and unselective reaction towards a complex mixture of species (starting materials in equilibrium with other species, see ESI†) that we were not able to isolate from each other in the solid-state. Among them, we can assume that the 1:1 adduct is partly formed. On the opposite, the stoichiometric reaction of Al(C₆F₅)₃(tol) with $[Cr(dmpe)_2(N_2)_2]$ cleanly produced a new 1:1 adduct 7_{Al} in good yields (Scheme 1, bottom). Spectroscopic and crystallographic parameters of 7_{Al} are nearly identical to those of tungsten and molybdenum analogues 1_{Al} and 2_{Al} (see Fig. 3 and Table 3)

DFT investigation on the N-N-LA angle

and Al-N-N angles in particular).

Chemical Science

To shed light into these results, DFT calculations at the BP86/def2-TZVP level of theory were employed, including implicit solvation and dispersion corrections, starting from the crystal structures of the BCF and AlCF adducts. One explicit solvent molecule was added to the molecular models due to the aforementioned greater stability of AlCF in a tetrahedral environment; this is required for the analysis of the thermodynamics behind the LA binding.

showing a similar N_2 activation degree (close N-N distances and $N \equiv N$ IR stretches) and AlCF coordination (close Al-N distances

The potential energy surface (PES) minima found upon geometry relaxation match well with experiment: M-N₁ and N₂-LA bonds were only ca. 0.050 Å longer than the experimental ones and other deviations were even smaller. The N₁-N₂-LA angles obtained for the computed structures of AICF and BCF adducts were 170° and 148°, respectively. A detailed comparison of the computational and experimental structural and spectroscopic features is included in the ESI (Tables S5 and S6).† To further elucidate the PES regarding the binding angle of the LAs, constrained geometry optimisations with varying N-N-LA angles (148° to 172°) were carried out for both LA adducts (Fig. 2). The N≡N-B angle is in fact extremely flexible: in the case of the least sterically impeded adduct, we observe the energy minimum at ca. 150° (in agreement with experimental data) and a small dent close to 165°, separated by less than 0.5 kcal mol⁻¹. The latter is not a local minimum as it is due to a ca. 10° rotation of one ethyl phosphine substituent. The increase in energy along the bending motion is, overall, meagre, with an energetic cost of less than 1 kcal mol^{-1} . For the AlCF 1: 1 adduct, in contrast, a continuous and steeper increase in energy is observed as the N≡N-LA angle is decreased.

There is a marginal stabilisation of the frontier occupied orbitals in both adducts as the angle is bent from 148° to 172°

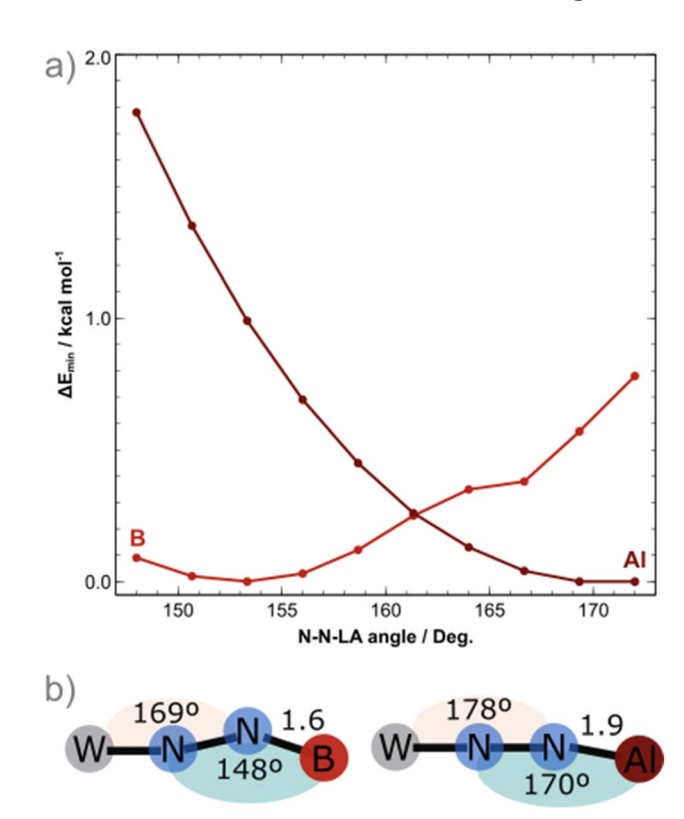


Fig. 2 (a) Potential energy surface along the N-N-Lewis acid angle coordinate for the AlCF (crimson) and BCF (red) 1:1 adducts, energies reported relative to PES minimum; and (b) relevant angles of the optimized structures.

(Fig. S93†), suggesting that the differing angles obtained in the crystal structures are not rooted in electronic structure stabilisation effects but are instead mainly due to steric hindrances. Note that for the N \equiv N-LA angle to bend (blue in Fig. 1b), a simultaneous bending of the M-N₁ \equiv N₂ angle (peach, in Fig. 1b) by 9° occurs to better accommodate the LA around the phosphine ligand arms. This is true for both LAs.

Influence of the atmosphere: N2 vs. Ar

It is important to mention that for adducts in the depe and dmpe series we observed the same reactivity whether working under dinitrogen or argon. Nevertheless, we noticed significant divergences for the dppe series. Indeed, when using B(C₆F₅)₃, our group had previously observed the elimination of one dinitrogen molecule during the reaction leading to the formation of [M(dppe)₂(μ-N₂)B(C₆F₅)₃] adducts where the apical site (left vacant by N₂ dissociation) is occupied by an agostic interaction with an ortho hydrogen of one of the phenyl groups in the solidstate.39 This process occurred under argon (Scheme 2, middle). Under dinitrogen, we noticed the same reactivity for trans- $[Mo(dppe)_2(N_2)_2]$ (i.e. loss of one of the N_2 ligands) but the stoichiometric treatment of trans- $[W(dppe)_2(N_2)_2]$ with BCF leads, after one night, to a mixture of [W(dppe)₂(μ-N₂)B(C₆F₅)₃] 3_B and trans- $[W(dppe)_2(N_2)(\mu-N_2)B(C_6F_5)_3]$ 5_B in a 31:69 3_B:5_B ratio, respectively. Of note, species 5_B was observed in solution but we did not succeed to isolate it (see Scheme 1, top left, and ESI†).

Edge Article

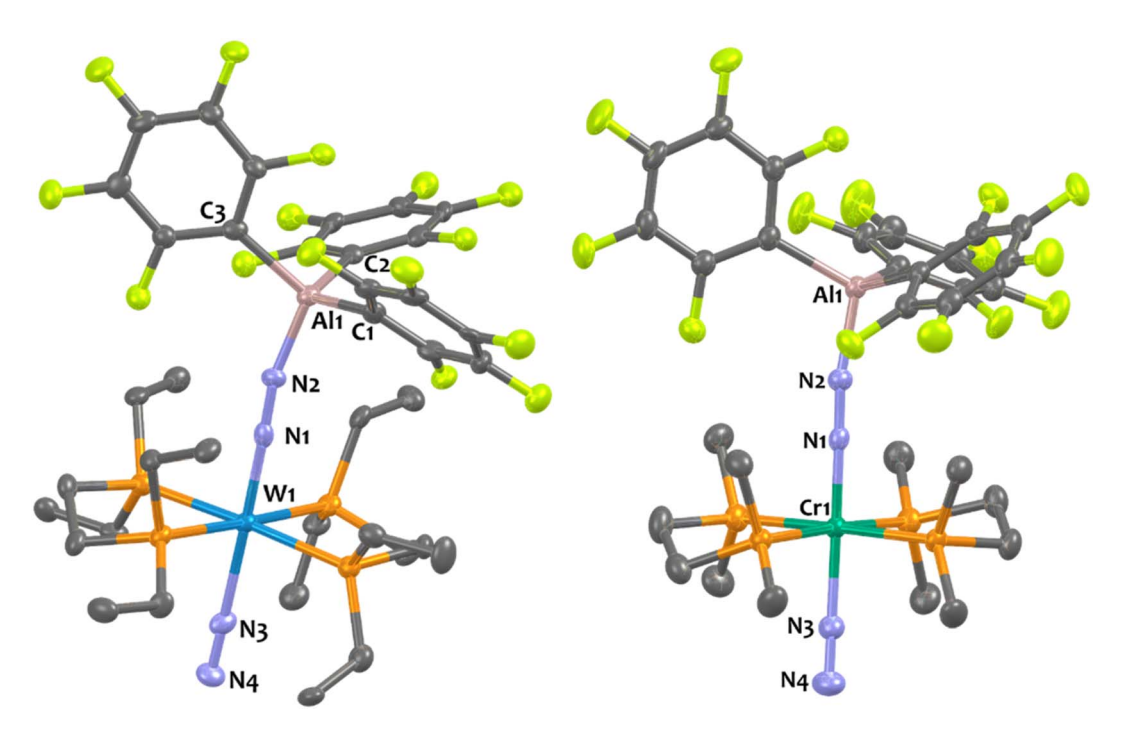


Fig. 3 Solid-state structures of 1_{Al} and 7_{Al} . Ellipsoids are represented with 30% probability. Hydrogen atoms have been omitted for clarity. Two independent molecules were found in the asymmetric unit (Z' = 2) of $\mathbf{1}_{Al}$ but one of them has been omitted for clarity. Selected bond distances (Å) and angles (°) have been averaged between both independent molecules for 1_{Al} : $Al_1 - N_2 1.816(7)$, $W_1 - N_1 1.855(2)$, $W_1 - N_3 2.113(2)$, $N_1 - N_2 1.203(6)$, and $N_1 - N_2 1.816(7)$, $N_2 - N_3 1.816(7)$, $N_3 - N_4 \ 1.114(1), \ W_1 - N_1 - N_2 \ 178.6(6), \ W - N_3 - N_4 \ 177.2(6), \ N_1 - W_1 - N_3 \ 177.3(6), \ N_1 - N_2 - Al_1 \ 168.3(6). \ For \ 7_{Al}: \ Al_1 - N_2 \ 1.8473, \ Cr_1 - N_1 \ 1.7507, \ Cr_1 - N_3 \ 177.3(6), \ N_1 - N_2 - Al_1 \ 168.3(6). \ For \ 7_{Al}: \ Al_1 - N_2 \ 1.8473, \ Cr_1 - N_1 \ 1.7507, \ Cr_2 - N_3 \ 1.7507, \ Cr_3 - N_3 \ 1.7507$ $1.9766,\ N_1-N_2\ 1.177(2),\ N_3-N_4\ 1.100(3),\ N_3-Cr_1-N_1\ 177.47(7),\ N_2-N_1-Cr_1\ 178.55(2),\ N_4-N_3-Cr_1\ 178.02(18),\ N_1-N_2-Al_1\ 170.26(2).$

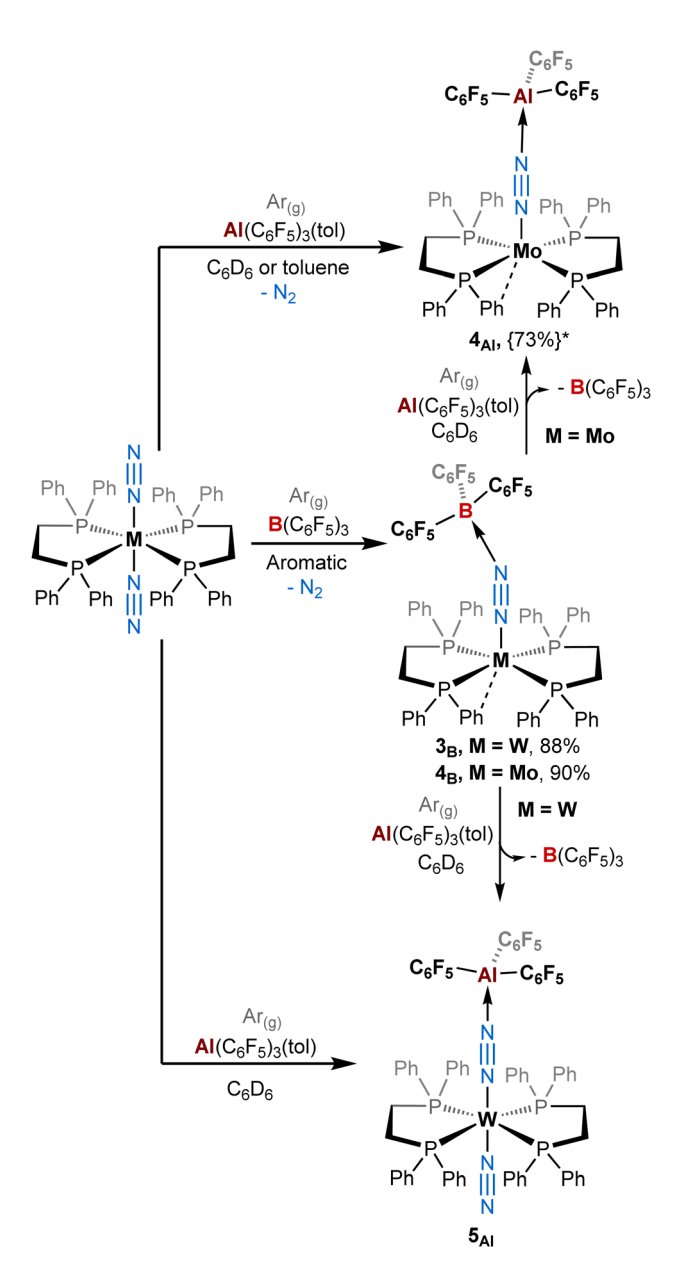
By contrast, the reaction of Al(C₆F₅)₃ with trans- $[M(dppe)_2(N_2)_2]$ (M = Mo and W) does not promote the elimination of N2 when working under a dinitrogen atmosphere. This leads instead to a similar reactivity to that of the depe series i.e. the formation of products 5_{Al} and 6_{Al} where the terminal N2 stays bonded to the metal centre (Scheme 1). Under an inert atmosphere of argon, the stoichiometric treatment of AICF with trans-[Mo(dppe)₂(N₂)₂] leads predominantly (73%) NMR yield, see ESI†) to the formation of the aluminium analogue of $\mathbf{4}_{\mathbf{B}}$, [Mo(dppe)₂(μ -N₂)AlCF] $\mathbf{4}_{\mathbf{Al}}$, in which the second dinitrogen ligand is lost during the reaction (Scheme 2, top). Identity of adduct 4_{Al} is successfully established by XRD studies. It should be noted, however, that the quality of XRD data was not good enough to discuss the metrical parameters in great detail but confirmed the atom connectivity and loss of one N2 ligand (see ESI†).

Surprisingly, changing from Mo to W drastically impacts this chemistry since the 1:1 reaction of trans- $[W(dppe)_2(N_2)_2]$ with AICF under argon does not trigger N2 dissociation and instead promotes the quantitative formation of 5_{Al} as under a dinitrogen atmosphere (see Scheme 2, bottom, and ESI†). This highlights the sensitivity of these species towards the retention of their second N2 ligand, depending whether the reaction medium is N2-saturated or not. We assumed that formation of adducts 3-4 involves first the formation of 5-6 as intermediates (coordination of the LA at the distal N), which can then lose their terminal N₂ ligand depending on the LA and the atmosphere. In this case, this second step is more feasible (in ascending order) for $4_B > 3_B > 4_{Al} > 3_{Al}$. This translates into Moand/or B-containing species having a greater tendency to labilise the trans-N2 ligand. Spectroscopic and crystallographic data of 3-4 vs. 5-6 revealed distinct features (Table 3). The IR μ -N \equiv N stretching mode is shifted to lower wavenumbers for adducts 3-4 vs. 5-6 and the bridging N-N distances are elongated in adducts 3-4 vs. 5-6. Therefore, the elimination of the terminal dinitrogen molecule induces a stronger polarisation of the M-N≡N-LA fragment (3_B, 4_B vs. 5_{Al} and 6_{Al}). Notably, comparable crystallographic data between 5_{Al} , 6_{Al} and 1_{Al} , 2_{Al} are found when it comes to the LA- N_2 distance and N_1 - N_2 -LA angle *i.e.* a short Al-N separation and a nearly linear Al-N≡N array, again contrasting with the boron adducts 3_B and 4_B featuring bent B-N≡N angles (see Table 3).

Also, similarly to the depe series, the stronger affinity of N₂ metal complexes for AICF vs. BCF in the dppe series was verified experimentally by treating the BCF adducts 3_B-4_B with one equivalent of AICF producing instantly (whether working under argon or dinitrogen) the aluminium adducts 4_{Al} , 5_{Al} , and 6_{Al} and free BCF (see Scheme 1, left, Scheme 2, and ESI†). These reactions demonstrate the stronger affinity of AICF vs. BCF for the dinitrogen ligand.

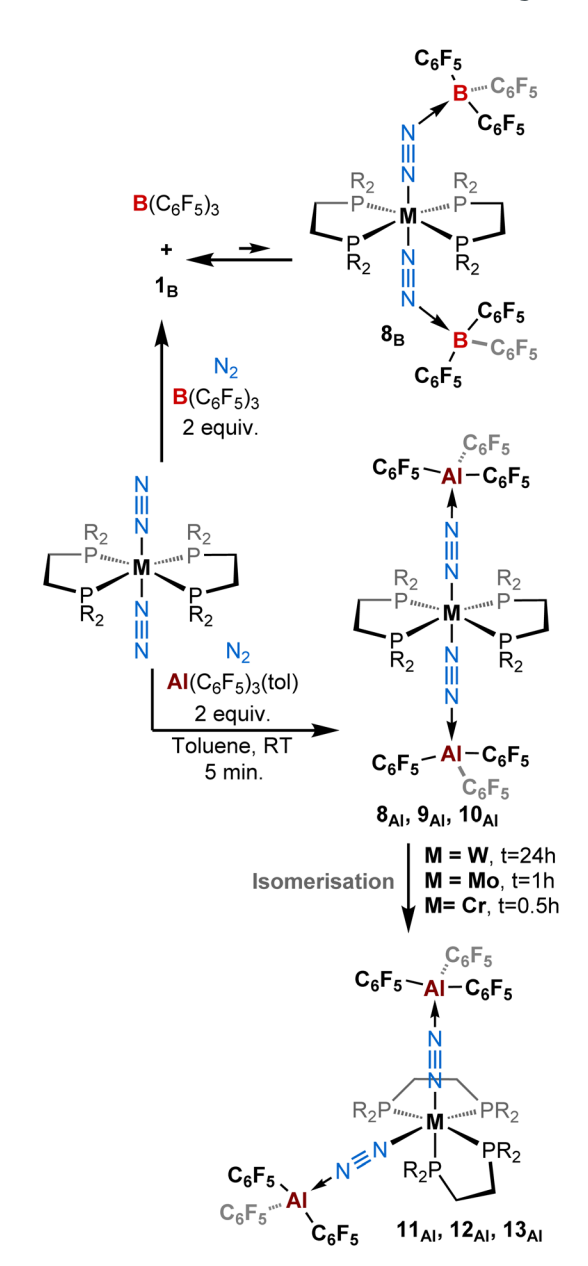
Syntheses of 2:1 adducts

Since we employed bis(dinitrogen) complexes as Lewis base partner, we were curious to know whether the reaction of $[ML_2(N_2)_2]$ with two equivalents of the Lewis acid (AlCF or BCF) could provide 2:1 adducts. When we added two equivalents of $B(C_6F_5)_3$ to $[M(depe)_2(N_2)_2]$ (M = Mo, W) we noticed an



Scheme 2 Reactivity of $ML_2(N_2)_2$ (M = W, Mo; L = dppe) complexes with $B(C_6F_5)_3$ and $A((C_6F_5)_3$ (tol) under an argon atmosphere. {The yield in brackets followed by a star*} represents the NMR yield. The other complexes (L = depe or dmpe) reacted similarly as under a dinitrogen atmosphere (see Scheme 1).

immediate colour change from orange-brown to deep purpleblue. While in the case of molybdenum, NMR analyses suggested some degradation occurring upon addition of the second equivalent of **BCF**, the spectra recorded when the W species was employed suggests the formation of a new putative complex $\mathbf{8_B}$ (see Scheme 3, top, and Table 2). This is evidenced by a gain in symmetry as indicated by undifferentiated alkyl protons in the 1 H NMR spectrum, as opposed to $\mathbf{1_B}$ (see ESI†). However, we also cannot exclude that such 1 H NMR spectrum results from signal coalescence of $\mathbf{1_B}$ due to a concentration phenomenon as already observed in the case of $\mathbf{1_{Al}}$ (Fig. S1–S3 and S40†). This



Scheme 3 Reactivity of $[ML_2(N_2)_2]$ (M=W, Mo, Cr; L= depe, dppe, dmpe) complexes with (top) two equivalents of $B(C_6F_5)_3$ and (bottom) two equivalents of $Al(C_6F_5)_3$ (tol) under a dinitrogen atmosphere.

could explain why the ^{31}P NMR spectrum showed no change with respect to the mono adduct $\mathbf{1_B}$ ($\delta=34.7$ ppm). Surprisingly, only two large signals are observed in ^{19}F NMR, contrasting with the well-resolved multiplets characterizing *ortho*, *meta* and *para* fluorine resonances in $\mathbf{1_B}$. This may suggest either a fluxional behaviour of $\mathbf{8_B}$ or that a fast $\mathbf{1_B}+\mathbf{BCF} \rightleftharpoons \mathbf{8_B}$ equilibrium takes place at room temperature. Measuring ^{1}H and ^{19}F NMR at low temperature (down to -60 °C) resulted in de-coalescence of the signals. In particular, broad resonances, which chemical shifts match those of $\mathbf{1_B}$ and free BCF, are found in the ^{19}F NMR spectrum, pointing to an equilibrated mixture. Shoulders on the peaks of the *para* and *meta* fluorine of $\mathbf{1_B}$ might be assigned to the two-fold adduct $\mathbf{8_B}$ (Scheme 1, top-right, and Fig. S40†).

Edge Article Chemical Science

Table 2 Description of the two-fold adducts

Compound	LA^a	M	R	Config.	N ₂ motifs	Yield (%)	
8 _{Al}	AlCF	W	Et	trans	2× μ-N ₂	96	
8 _B	BCF	W	Et	trans	$2 \times \mu$ - N_2	$n.i.^b$	
9_{Al}	AlCF	Mo	Et	trans	$2 \times \mu$ - N_2	n.i.^b	
10_{Al}	AlCF	Cr	Me	trans	$2 \times \mu$ - N_2	n.i. ^b	
11 _{Al}	AlCF	W	Et	cis	$2 \times \mu$ - N_2	77	
12 _{Al}	AlCF	Mo	Et	cis	$2 \times \mu$ - N_2	94	
13 _{Al}	AlCF	Cr	Me	cis	$2\times$ $\mu\text{-}N_2$	77	

^a LA = Lewis acid. ^b n.i. = not isolated.

Unfortunately, our attempts to isolate such a two-fold adduct were unsuccessful: crystals of $\mathbf{1}_B$ were systematically collected from the purple solutions.

Gratifyingly, treatment of trans- $[M(depe)_2(N_2)_2]$ (M=Mo,W) and trans- $[M(dmpe)_2(N_2)_2]$ (M=Cr) with two equivalents of AlCF-toluene instantly triggered a quantitative reaction characterised by a colour change from reddish $(ML_2(N_2)_2)$ starting materials) to blue azure/greenish within seconds. We attributed this colour change to the formation of a 2:1 adduct with a trans-configuration – species $\mathbf{8}_{Al}$ (M=W), $\mathbf{9}_{Al}$ (M=Mo), and $\mathbf{10}_{Al}$ (M=Cr) (Scheme 3, Table 2, and Fig. 4, top). With time, we noticed an additional colour change from blue/green to brown/orange corresponding to the formation of another 2:1 adduct this time with a cis-configuration, namely products $\mathbf{11}_{Al}$ (M=W), $\mathbf{12}_{Al}$ (M=Mo), and $\mathbf{13}_{Al}$ (M=Cr) (Scheme 3, bottom, and Fig. 4, bottom).

In the case of tungsten, intermediate 8_{AI} is stable enough (for one or two hours at room temperature) so that we succeeded to

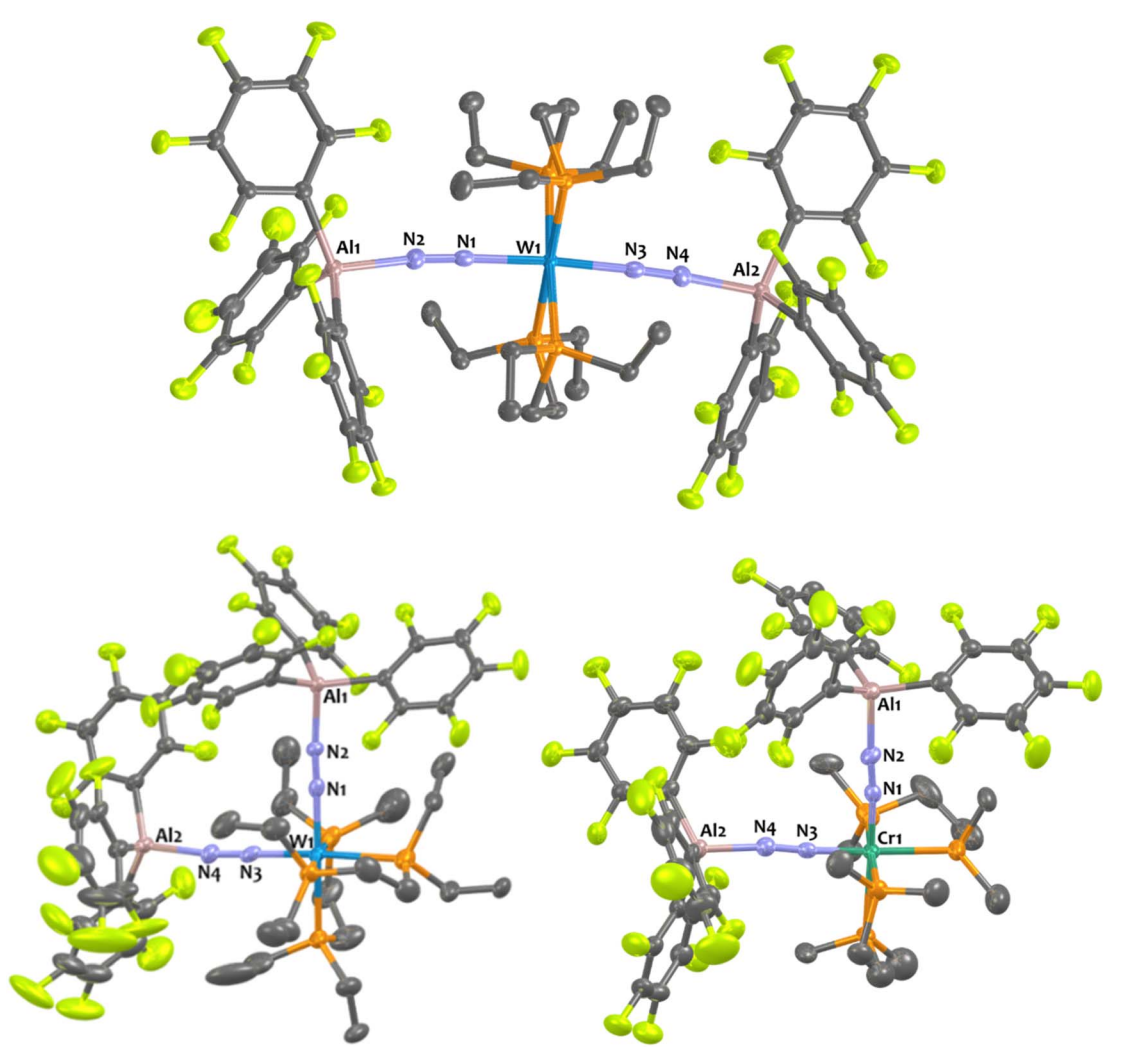


Fig. 4 Solid-state structures of $\mathbf{8}_{Al}$, $\mathbf{11}_{Al}$ and $\mathbf{13}_{Al}$. Ellipsoids are represented with 30% probability. Hydrogen atoms have been omitted for clarity. Two independent molecules were found in the asymmetric unit (Z'=2) of $\mathbf{11}_{Al}$ and $\mathbf{13}_{Al}$ but one of them has been omitted for clarity. Selected bond distances (Å) and angles (°) have been averaged between both independent molecules for $\mathbf{11}_{Al}$ and $\mathbf{13}_{Al}$. For $\mathbf{8}_{Al}$: Al₁-N₂ 1.927(2), Al₂-N₄ 1.919(2), W₁-N₁ 1.964(2), W₁-N₃ 1.956(3), N₁-N₂ 1.113(3), N₃-N₄ 1.114(3), N₃-W₁-N₁ 174.13(7), N₂-N₁-W₁ 176.88(2), N₄-N₃-W₁ 177.09(2), N₁-N₂-Al₁ 168.64(2), N₃-N₄-Al₂ 175.22(2). For $\mathbf{11}_{Al}$: Al₁-N₂ 1.901(4), Al₂-N₄ 1.894(0), W₁-N₁ 1.919(9), W₁-N₃ 1.901(0), N₁-N₂ 1.144(6), N₃-N₄ 1.156(6), W₁-N₁-N₂ 175.5(4), W₁-N₃-N₄ 175.8(4), N₁-W₁-N₃ 89.20(7), Al₁-N₂-N₁ 175.7(9), Al₂-N₄-N₃ 168.7(4). For $\mathbf{13}_{Al}$ Al₁-N₂ 1.884(6), Al₂-N₄ 1.899(0), Cr₁-N₁ 1.784(2), Cr₁-N₃ 1.778(9), N₁-N₂ 1.156(1), N₃-N₄ 1.157(1), Cr₁-N₁-N₂ 175.6(9), Cr₂-N₃-N₄ 176.0(9), N₁-Cr₁-N₃ 89.19(2), Al₁-N₂-N₂ 170.8(4), Al₂-N₄-N₃ 172.0(0).

Table 3 Relevant structural and spectroscopic parameters (distances (Å), angles (°), wavenumbers (cm⁻¹), chemical shift (ppm)) of the aluminium and boron adducts

Adduct	δ 31 P NMR a	v_1 (μ - N_2)	ν_2 (N ₂)	N_1 – N_2	N ₃ -N ₄	N_2 -LA ^b	N_4 – LA^b	$M-N_1$	$M-N_3$	N_1 - M - N_3	N_1 - N_2 - LA^b	N_3 - N_4 - LA^b
1_{Al}	34.6	1778	2088	1.204	1.114	1.817	_	1.855	2.113	177.4	168.4	_
1_{B}	34.7	1767	2076	1.181	1.082	1.549	_	1.909	2.015	175.7	148.4	_
2_{Al}	52.6	1790	2137	1.168	1.103	1.842	_	1.869	2.128	177.7	167.8	_
2_{B}	53.0	1789	2120	1.175	1.093	1.562	_	1.894	2.129	176.3	150.9	_
3_B	69.2	1717	_	1.212	_	1.571	_	1.841	_	_	140.3	_
4_{Al}	70.9	_	_	_	_	_	_	_	_	_	_	_
4_{B}	73.1	1744	_	1.197	_	1.568	_	1.841	_	_	141.5	_
5_{Al}	45.4	1773	2121	1.181	1.090	1.865	_	1.885	2.108	177.2	169.3	_
6_{Al}	63.1	1786	2161	1.174	1.094	1.876	_	1.894	2.139	173.8	176.6	_
7_{Al}	62.3	1802	2122	1.177	1.100	1.847	_	1.751	1.977	177.5	170.3	_
8 _{Al}	31.0	1808	_	1.113	1.114	1.927	1.919	1.964	1.956	174.1	168.6	175.2
11 _{Al}	28.6, 16.6	1903, 1802	_	1.145	1.157	1.901	1.894	1.920	1.901	89.2	175.8	168.7
12 _{Al}	44.4, 29.2	1927, 1821	_	1.148	1.138	1.892	1.907	1.910	1.921	88.6	173.9	170.7
13 _{Al}	_	1948, 1833	_	1.156	1.157	1.885	1.899	1.784	1.779	89.2	170.8	172.0
15 _{Al}	-18.8, -22.1, -25.5	1776	2037	_	_	_	_	_	_	_	_	_
16 _{Al}	-24.3, -26.5	1901, 1804	_	1.149	1.150	1.915	1.891	1.917	1.906	91.3	168.5	179.1

^a Recorded in C_6D_6 . ^b LA = Lewis acid.

isolate it and analyse it by IR, XRD, and NMR. Then, 8_{Al} is progressively (within one day) converted into product 11_{Al}. However, intermediates 9_{Al} (M = Mo) and 10_{Al} (M = Cr) evolved within minutes towards products 12Al and 13Al, precluding their isolation (see ESI† for further details). The trans geometry of intermediate 8_{Al} is first evidenced by its ¹H NMR spectrum that exhibits 3 centrosymmetric signals ($\delta = 1.44$, 1.13, and 0.68 ppm) and by its ³¹P NMR spectrum that displays a shielded pseudo-triplet (${}^{1}J_{W-P} = 141 \text{ Hz}$) at $\delta = 31.0 \text{ ppm}$ (vs. 34.6 ppm for $\mathbf{1}_{Al}$). This configuration is confirmed by its structure in the solidstate (Fig. 4, top). Here, the $Al_1-N_2-N_1-W_1-N_3-N_4-Al_2$ atoms are almost perfectly aligned. Also, the coordination of a second AICF moiety imparts a significant shortening of the N-N bonds $(1.11 \text{ Å vs. } 1.20 \text{ Å in } \mathbf{1}_{Al})$ and elongation of the W-N₁ (1.96 Å vs.)1.86 Å in $\mathbf{1}_{Al}$) and Al-N (1.92 Å vs. 1.82 Å in $\mathbf{1}_{Al}$) bonds (see Table 3) showing a decreased activation of the bridging dinitrogen fragments. These features are verified by IR where the ATR spectrum of 8_{Al} displays a single bridging N₂ stretch at higher wavenumber to that of $\mathbf{1}_{Al}$ (1808 vs. 1778 cm⁻¹). Based on these data, we propose a formal bridging Al-N≡N-M depiction. The cis arrangement of products 11AI and 12AI is first demonstrated by NMR spectroscopy as their ¹H NMR spectra display asymmetrical depe resonances (see Fig. S44 and S54†) and their ³¹P NMR spectra feature two triplets $\binom{2}{J_{P-P}} = 6$ Hz and 14 Hz for 11_{Al} and 12_{Al}), each integrating for 2P (see Table 3 and ESI†). We could not analyse 13_{Al} (M = Cr, L = dmpe) by NMR spectroscopy as this species was not soluble in chemically compatible deuterated solvents (even ortho-dichlorobenzene). IR-ATR spectra of 11_{Al}, 12_{Al}, and 13_{Al} display two intense N≡N bands (see Table 3) assigned to symmetric and asymmetric N₂ stretches. Eventually, solid-state structures of 11_{Al}, 12_{Al}, and 13_{Al} (see Fig. 4-bottom and ESI†) confirmed the cis arrangement, with almost orthogonal N₁-M-N₃ angles. Of note, an elongation of the N-N bond is observed for 11_{Al} when compared to the *trans* adduct 8_{Al} (1.152 Å vs. 1.113 Å, respectively).

DFT investigation on the 2:1 adduct formation

DFT calculations show that sequential binding of two equivalents of **BCF** or **AlCF** is thermodynamically favourable (Fig. 5), although binding of the second LA is associated with a relatively lower stabilisation of the adduct as may be expected from the *trans* effect. The individual contributions to the Gibbs energies can be found in the ESI, Tables S7 and S8.†

The **AICF** adducts are lower in relative energy than the **BCF** analogues. Conversion from *trans* to *cis* adducts was observed and indeed the *cis* isomeric form is shown to be more stable by 3.0 kcal mol⁻¹ over the *trans* 2:1 adduct. We analysed the MO diagrams of the **AICF** adduct series to rationalise the degree of dinitrogen activation observed (Fig. 6). The complete frontier MO diagram as well as the depiction of the orbitals for the bare tungsten depe complex can be found in the ESI (Fig. S92).†

The binding of LAs to the terminal atom of the nitrogen ligand has been shown to stabilise π^* interactions in the N-N

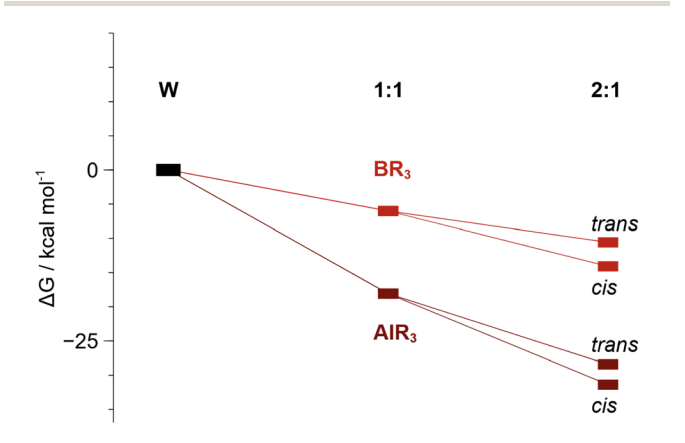
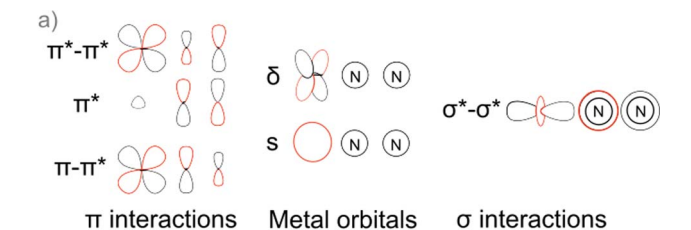


Fig. 5 Relative Gibbs energies (kcal mol^{-1}) of 1:1 (1_B and 1_{Al}) and 2:1 adduct formation. The cis isomer is more stable than the trans by ca. 3 kcal mol^{-1} .

Edge Article



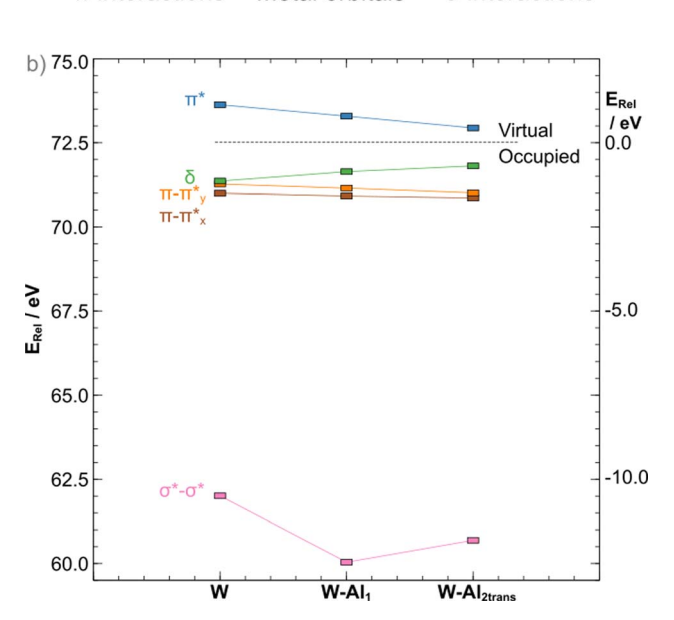


Fig. 6 (a) 2D depiction of the orbitals involved in the "push–pull" activation and metal s orbital used as reference and (b) MO diagram for the Al series of adducts (blue: LUMO/LUMO+1 average; green: HOMO; orange: HOMO–1, brown: HOMO–2, pink: σ antibonding interaction within the bridge). Orbital energies are plotted relative to the tungsten s orbital and thus all are positive (left vertical axis). Energies relative to proximally the midpoint of the HOMO/LUMO gap shown on the right vertical axis. Nomenclature of the orbitals considers symmetry.

bridge, resulting in bond25 weakening. In the case of the depe complexes, the same is observed when the formation of the 1:1 adduct occurs as a ca. 0.10 eV stabilisation from the bare complex to the AICF 1 : 1 adduct ($\nu_{N-N} = 1778 \text{ cm}^{-1}$) is observed. However, in apparent contradiction to experimental results (ν_{N-} $_{\rm N}$ = 1808 cm⁻¹ measured for the 2:1 trans adduct), a further ca. 0.08 eV stabilisation is noted upon binding of the second LA. As we have shown in previous work, 45 an analysis of the π interactions is insufficient to explain dinitrogen activation in such complexes. A concomitant destabilisation (0.65 eV) of the σ^* - σ^* orbital is observed that greatly exceeds the π stabilisation, explaining the increase in N-N stretching frequency (from the computed 1864 cm⁻¹ in W-Al₁ to 1880 cm⁻¹ in W-Al_{2trans}). The more stable cis adduct showed a slightly decreased bond strength ($\nu_{N-N} = 1802 \text{ cm}^{-1}$). The MO diagram for the cis 2:1 adduct shows a further 0.21 eV destabilisation of the σ^* - σ^* orbital, which should result in a stronger dinitrogen bond. It is not the case here, however, as the different coordination geometry allows for mixing of the metal d orbital that would form the δ MO in the *trans* adducts with the π orbitals of the dinitrogen bridge (Fig. 7). Therefore, the nature of the HOMO –

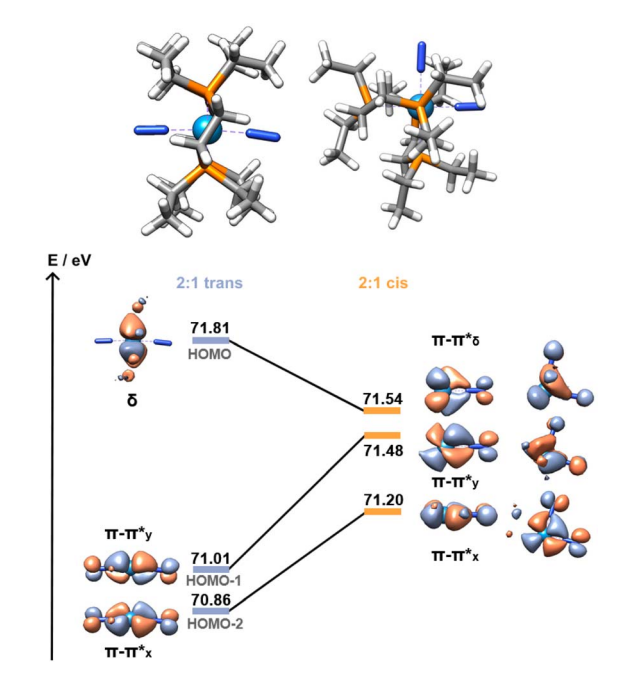


Fig. 7 $\,$ Cis (11_{Al}) vs. trans (8_{Al}) frontier orbitals (HOMO to HOMO-2). AICF omitted for clarity. Orbitals of the cis isomer are shown in side and top views.

a metal-centred orbital in the *trans* isomer – is significantly modified, forming an additional π – π * interaction in the *cis* isomer. This yields a total population of 6 electrons in N–N antibonding frontier orbitals instead of 4, leading to a greater overall activation of the N–N bond. The higher extent of the overlap between the metal and ligand orbitals is also likely responsible for the greater stability of this form.

Case of a monophosphine-supported W-N2 complex

To get more insights about the divergent chemical behaviours of AICF vs. BCF towards bis-dinitrogen complexes, we also investigated their reactivity with cis- $[ML'_4(N_2)_2]$ species (M = Mo)or W, L' = dimethylphenylphosphine). Stoichiometric treatment of BCF with cis-[WL'₄(N₂)₂] leads to the partial abstraction of one PMe₂Ph ligand to form a BCF-phosphine adduct species 14 - (Scheme 4-top left) with a complex mixture of species (see ESI†) that we were not able to identify (except some remaining starting dinitrogen complex). From this experiment we concluded that adjunction of the Lewis acid mainly triggered decomposition. Furthermore, this highlights the ease for **BCF** to dissociate a monophosphine ligand suggesting its stronger affinity for PMe₂Ph vs. N₂. On the opposite, using similar conditions to that of the $[M(depe)_2(N_2)_2]$ series, the reaction of **AICF** with cis-[ML $'_4$ (N $_2$) $_2$] (M = W) produces new LA-dinitrogen adducts - products 15Al and 16Al (Scheme 4, bottom). First clues about the identity of the mono adduct 15AI is evidenced by NMR spectroscopy. Indeed, its ³¹P NMR spectrum displays three signals at chemical shifts of -18.8, -22.1, and -25.5 ppm integrating respectively for 1, 2 and 1 phosphorus nuclei. This NMR signature suggests that 15_{Al} is cis-[W(PMe₂Ph)₄(N₂){μ-N₂-Al(C₆F₅)₃}] having one terminal dinitrogen motif and one

$$\begin{array}{c} \textbf{B}(C_6F_5)_3\\ \hline C_6D_6, RT \\ \hline \\ \textbf{Ph} \\ \hline \\ \textbf{AI}(C_6F_5)_3(tol)\\ \hline \\ \textbf{2 equiv.} \\ \hline \\ \textbf{Toluene, RT} \\ \hline \\ \textbf{C}_6F_5\\ \hline \\ \textbf{C}_6F_5\\ \hline \\ \textbf{C}_6F_5\\ \hline \\ \textbf{AI}(C_6F_5)_3(tol)\\ \hline \\ \textbf{2 equiv.} \\ \hline \\ \textbf{Toluene, RT} \\ \hline \\ \textbf{C}_6F_5\\ \hline \\ \textbf{C}_6F_5\\ \hline \\ \textbf{AI}(C_6F_5)_3(tol)\\ \hline \\ \textbf{2 equiv.} \\ \hline \\ \textbf{Toluene, RT} \\ \hline \\ \textbf{C}_6F_5\\ \hline \\ \textbf{AI}(C_6F_5)_3(tol)\\ \hline \\ \textbf{2 equiv.} \\ \hline \\ \textbf{16_{AI}}, 91\% \\ \hline \\ \textbf{2 equiv.} \\ \hline \\ \textbf{2 equiv.} \\ \hline \\ \textbf{3 equiv.} \\ \hline \\ \textbf{3 equiv.} \\ \hline \\ \textbf{4 equiv.} \\ \hline \\ \textbf{4$$

Scheme 4 Reactivity of $[M(PMe_2Ph)_4(N_2)_2]$ (M = W or Mo) complexes with (top) $B(C_6F_5)_3$ and (bottom) $Al(C_6F_5)_3$ (tol).

bridging dinitrogen fragment. These above aspects are confirmed by IR spectroscopy where coordination of one **AlCF** molecule at one distal nitrogen induces an averaged bath-ochromic shift of $-171~\rm cm^{-1}$ of the μ -N \equiv N IR band $-1776~\nu s$. 1947 cm $^{-1}$ in cis-[W(PMe₂Ph)₄(N₂)₂]— and an averaged hypsochromic shift of +89 cm $^{-1}$ of the terminal N \equiv N stretching mode $-2037~\nu s$. 1947 cm $^{-1}$ in cis-[W(PMe₂Ph)₄(N₂)₂]. Unfortunately, despite the good purity of 15_{Al} verified by elemental and spectroscopic analysis, our attempts to get single crystals were unsuccessful.

Addition of two equivalents of $Al(C_6F_5)_3(tol)$ on *cis*-[W(PMe₂Ph)₄(N₂)₂] produced a new two-fold adduct $\mathbf{16_{Al}}$ —*cis*-[W(PMe₂Ph)₄{ μ -N₂-Al(C_6F_5)₃}₂]— that was fully characterised in solution and in the solid-state. Spectroscopic and crystallographic data of $\mathbf{16_{Al}}$ are very close to those of its congeners $\mathbf{11_{Al}}$ (M = W), $\mathbf{12_{Al}}$ (M = Mo), and $\mathbf{13_{Al}}$ (M = Cr), showing a cis geometry for the AlCF-(μ -N₂) fragments (see Table 3). Indeed, aside from their 31 P NMR chemical shifts, the IR and XRD data of $\mathbf{16_{Al}}$ ν s. $\mathbf{11_{Al}}$ are almost identical (see Table 3 and Fig. 8).

Electronic spectroscopy of the depe-supported W complexes

The recorded UV-vis absorption spectra of *trans*-[M(depe)₂(N₂)₂] (M = W and Mo) at 298 K display two types of bands, an intense transition (320–330 nm, $\varepsilon \approx 10^5 \ \text{M}^{-1} \ \text{cm}^{-1}$) assigned to metalto-ligand charge transfer (MLCT) involving a ligand phosphorus atom, and a less intense transition (440–500 nm, $\varepsilon \approx 10^3 \ \text{M}^{-1} \ \text{cm}^{-1}$) assigned to a ligand field (LF) d–d transition.

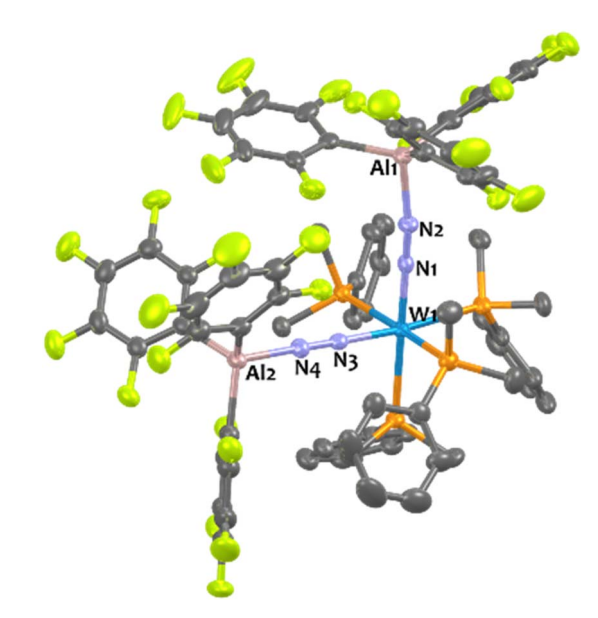


Fig. 8 Solid-state structure of ${\bf 16}_{\rm Al}$. Ellipsoids are represented with 30% probability. Hydrogen atoms have been omitted for clarity. Selected bond distances (Å) and angles (°): ${\bf Al_1}-{\bf N_2}$ 1.915(3), ${\bf Al_2}-{\bf N_4}$ 1.891(3), ${\bf W_1}-{\bf N_1}$ 1.917(3), ${\bf W_1}-{\bf N_3}$ 1.906(3), ${\bf N_1}-{\bf N_2}$ 1.149(4), ${\bf N_3}-{\bf N_4}$ 1.150(4), ${\bf W_1}-{\bf N_1}-{\bf N_2}$ 179.2(3), ${\bf W_1}-{\bf N_3}-{\bf N_4}$ 177.5(3), ${\bf N_1}-{\bf W_1}-{\bf N_3}$ 91.34(1), ${\bf Al_1}-{\bf N_2}-{\bf N_1}$ 168.5(3), ${\bf Al_2}-{\bf N_4}-{\bf N_3}$ 179.1(3).

The MLCT transition of the aluminium and boron adducts does not shift substantially ($\Delta\lambda$ < 3 nm) compared to that of the W starting complex (Fig. 9). However, their intensities are about two times lower compared to the W starting complex. We thus assign these energetically similar UV signatures to the

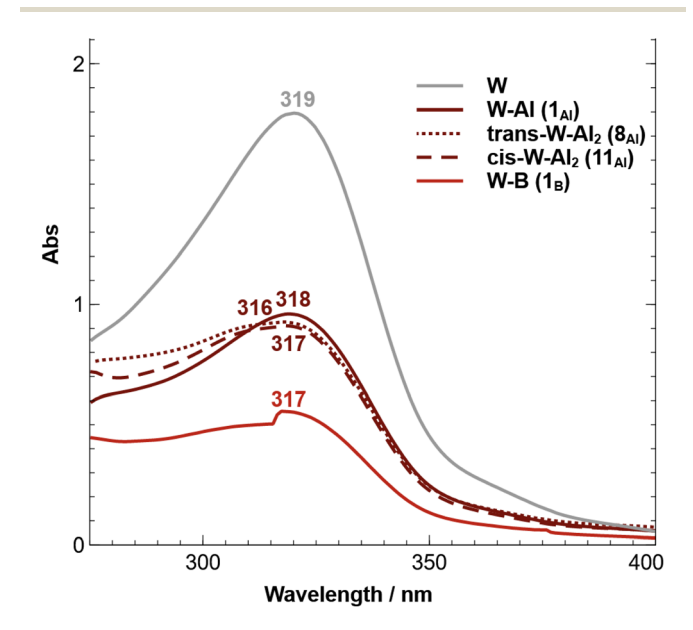


Fig. 9 Absorption spectra of trans-[W(depe)₂(N₂)₂] (W, grey line), trans-[W(depe)₂(N₂)(μ -N₂-Al(C₆F₅)₃)] (W-Al, crimson line), trans-[W(depe)₂((μ -N₂-Al(C₆F₅)₃)₂] (trans-W-Al₂, dotted crimson line), cis-[W(depe)₂((μ -N₂-Al(C₆F₅)₃)₂] (cis-W-Al₂, dashed crimson line), and trans-[W(depe)₂(N₂)(μ -N₂-B(C₆F₅)₃] (W-B, red line). The concentration of each sample is about 30 μ M.

Edge Article Chemical Science

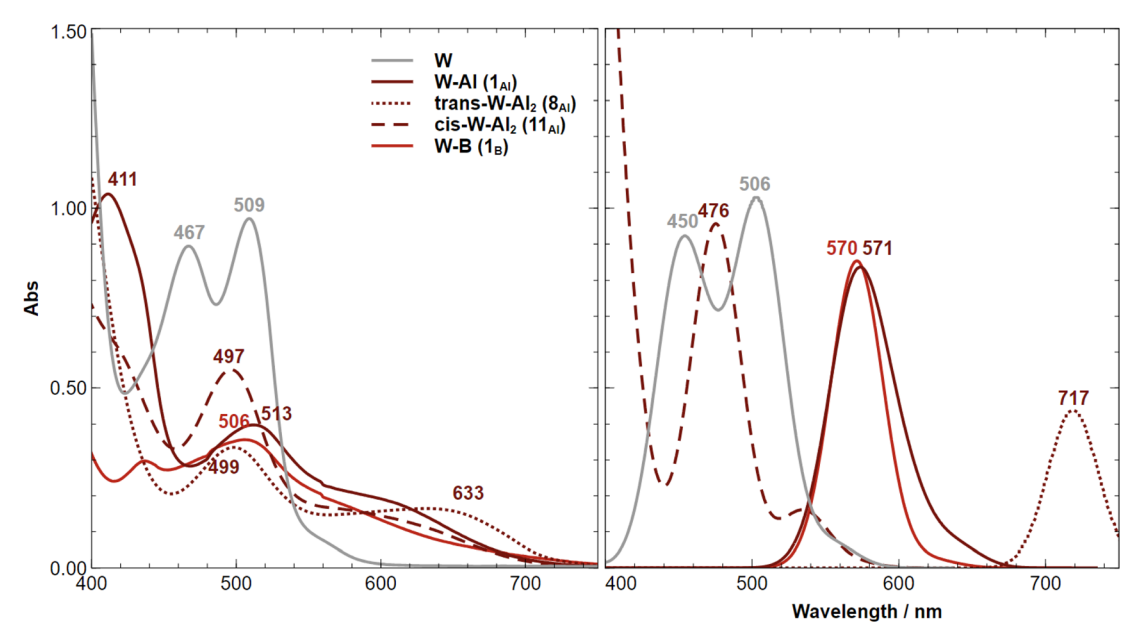


Fig. 10 Experimental (left) and computational (CAM-B3LYP, right) absorption spectra of trans-[W(depe)₂(N₂)₂] (W, grey line), trans-[W(depe)₂(N₂)(μ -N₂-Al(C₆F₅)₃)] (W-Al, crimson line), trans-[W(depe)₂($(\mu$ -N₂-Al(C₆F₅)₃)₂] (trans-W-Al₂, dotted crimson line), cis-[W(depe)₂($(\mu$ -N₂-Al(C₆F₅)₃)₂] (cis-W-Al₂, dashed crimson line), and trans-[W(depe)₂(N₂)($(\mu$ -N₂-B(C₆F₅)₃] (W-B, red line). The concentration of each sample is about 1000 μ M. A Lorentzian line broadening with FWHM of 8 was applied to the computed peaks.

chemical environment around the W-P that does not change substantially upon coordination of the LA (unlike the dinitrogen ligand where the coordination of AlCF or BCF takes place). Fig. 10 (left side) displays the visible spectra of each sample at a concentration of 10^{-3} M. The trans-W(depe)₂(N₂)₂ starting complex displayed two LF (d-d transitions) bands at λ_1 = 467 nm and λ_2 = 509 nm in agreement with literature data.⁸⁵ For the Al mono adduct (W-Al, crimson line) we observed a significant blue shift of the first band $-\lambda_1 = 411$ nm— and a small red shift of the second band $-\lambda_2 = 513$ nm. For the boron mono-adduct (red line), we observed a slight blue shift for the first and second bands ($\lambda_1 = 437$ nm, $\lambda_1 = 506$ nm). The Al double adducts of trans configuration display two new bands (crimson dotted line), one at a wavenumber of 499 nm and the other at a high wavenumber of 633 nm (this complex has a green-cyan colour). For the cis-double adduct, the spectrum displays a single maximum in the visible region at 497 nm. Note that for all the Al and B adducts, we noticed absorption in the [550-700 nm] spectral window (unlike the W starting complex where there is no absorption at all in this area).

Computing the electronic excitation spectra of transition-metal complexes with a high degree of quantitative accuracy is far from trivial. Revertheless TD-DFT calculations are key to provide understanding into the nature of the transitions responsible for the UV-vis bands. The peaks obtained *via* TD-DFT calculations (CAM-B3LYP/def2-TZVP) are in qualitative agreement with the recorded spectra, albeit being generally red shifted by *ca.* 30–60 nm, except for the bare tungsten complex in which an almost exact match is obtained. The monosubstituted adducts have almost overlapping spectra in both experiment and computations. Two peaks are observed in the

experimental UV spectrum of 11_{Al} (*trans*-W–Al₂, Fig. 10-left) while the computed one displays just one. A second, considerably red-shifted peak is visible in the computed spectrum at wavelengths greater than 750 nm (Fig. S97†). An analysis of the Natural Transition Orbitals (NTOs) shows, however, that these do not correspond to d–d transitions, but instead to low-lying MLCT transitions from the metal to both nitrogen ligands (Fig. 11). Such low-lying charge transfer transitions had already

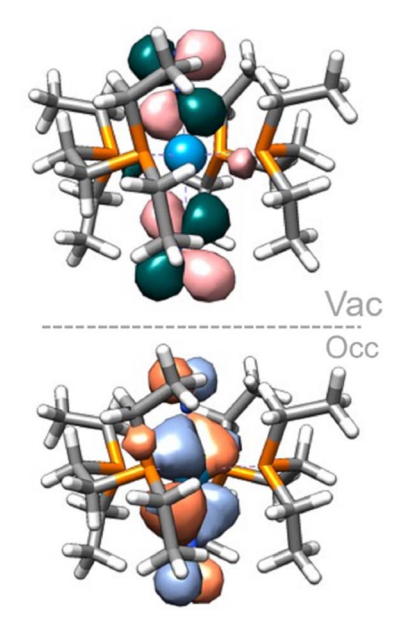


Fig. 11 NTOs (occupied – bottom, vacant – top) of the 450 nm band of the bare tungsten complex.

been identified in a Ru(II) complex⁸⁷ that has, like the compounds studied here, a ligand-based LUMO orbital. Remaining relevant NTOs as well as the calculated peaks and associated difference densities can be found in Fig. S94–S96.†

Conclusions

This work was motivated by previous results from our groups having thoroughly investigated, experimentally on the one hand, the coordination of tris(pentafluorophenyl)borane, BCF, to formally zerovalent group 6 bis(dinitrogen) complexes supported with phosphine ligands, and computationally on the other hand, the influence of LA binding to a dinitrogen ligand. This combined experimental/theoretical study explores similar chemistry employing tris(pentafluorophenyl)alane, AICF. The shift to a structurally comparable but more Lewis acidic species led to the isolation of related 1:1 adducts of an extensive family of dinitrogen complexes, including a chromium-based and monophosphine-based ones that could not be selectively formed when BCF was employed. A notable difference on the structural point of view is the linear N-N-Al vs. bent N-N-B motif that is explained by steric repulsion between the C₆F₅ groups with the ethyl substituents of the phosphines built up as a result of longer Al-C bonds.

Unlike BCF, AlCF makes robust two-fold µ-N2 adducts with the bis(dinitrogen) complexes. They form with an initial trans arrangement that evolves in solution to a more stable cis one with a rate depending on the metal (Cr > Mo > W). To the best of our knowledge, these compounds are the first examples of trinuclear heterometallic complexes formed by Lewis acid-base interaction exhibiting p and d elements. Among the handful of N₂-bridged trinuclear heterobimetallic species⁸⁸⁻⁹⁸ of general formula $M_1(\mu\text{-}N_2)M_2(\mu\text{-}N_2)M_1$ $(M_1 = \text{Cr},^{89} \text{Mo},^{95\text{-}97} \text{Re},^{92} \text{Fe},^{93}$ $Co_{3}^{90,91,93,94,98} M_{2} = Na_{3}^{95} Mg_{3}^{90,91,93-95,97,98} Ti_{3}^{89} Zr_{3}^{92,96} V_{3}^{96} Fe_{3}^{96}$ many are based on a low diversity of metal/metal couples, typically on magnesium/early transition metals pairs, as a result of a formally anionic dinitrogen complex formed by reduction with an alkaline or alkaline-earth metal. For the synthesis of dblock-only congeners, a general strategy consists in halide substitution by an electron-rich N₂ ligand, a transformation that accompanies with formal oxidation of the N2-ligated metal centre concomitant with reduction of N2. Here, the novelty of our bis(μ - η^1 : η^1 - N_2 -AlCF) specimens resides in the use of a pblock metal that interacts with neutral group 6 N2 complexes through Lewis acid-base pair formation, through straightforward syntheses (no redox state change, no by-products, and no workup). Note that this synthetic approach parallels a recent work published by Mazzanti and coworkers where they reported the coordination of f-elements (lanthanides and uranium) to an end-on dinitrogen iron complex leading to the formation of N2 bridged heterobimetallic adducts.99 Last but not least, the close proximity of the two activated dinitrogen motifs in these adducts (imparted by their *cis*-configuration) may pave the way towards new type of N2 reactivity. DFT calculations show that the diminished level of N2 activation in these systems, evidenced experimentally by comparison of IR and XRD data to those of the 1:1 adducts, can be interpreted by a destabilisation

of a σ -symmetric, W–N antibonding component of the W–N–N bonding. While the "bare" N_2 complexes, their 1:1 and *trans*-2:1 Lewis acid adducts have a HOMO of pure d character, in the *cis*-2:1 adducts this orbital overlaps with a π^* orbital of each N_2 ligands. This could result, in terms of reactivity, into a selective reactivity of the N_2 ligands towards electrophiles νs . the metal centre. From the bare $[W(\text{depe})_2(N_2)_2]$ complex to the two-fold aluminium adduct, substantial decrease of the HOMO–LUMO gap is noticed. In particular, the stabilized N_2 -centered LUMO should more easily accept electrons, suggesting Lewis acids could be co-activators for (electro) catalysed N_2 reduction.

Electronic spectroscopy was examined for the depesupported $W-N_2$ complex and its adducts both experimentally and computationally. This investigation suggests that the nature of the observed absorptions in the visible spectrum is an unusual low-lying MLCT involving N_2 -centered orbitals that significantly red-shifts upon LA coordination. This could have important implication for visible light-driven nitrogen fixation, and we are currently exploring the reactivity of LA-adducts of N_2 complexes towards this end.

Data availability

The datasets supporting this article have been uploaded as part of the ESI.† All the computational data have been uploaded (https://www.iochem-bd.org/handle/10/229000) onto the ioChem-BD platform (https://www.iochem-bd.org/) to facilitate data exchange and dissemination, according to the FAIR principles of OpenData sharing.

Author contributions

Conceptualization: A. S.; formal analysis: L. E., L. V., A. C., N. Q.; funding acquisition: A. S., V. K.; investigation L. E., A. C., N. Q., F. M.; methodology: L. E., A. C., N. Q., F. M., V. K., A. S.; project administration: V. K., A. S.; supervision V. K., A. S.; validation: L. E., F. M.; visualization: L. E., F. M.; writing – original draft: L. E., F. M.; writing – review & editing: V. K., A. S.

Conflicts of interest

There are no conflicts to declare.

Acknowledgements

L. E. and A. S. thanks the French Agence Nationale de la Recherche for funding (grant ANR-21-CE07-0003). N. Q. and A. S. are indebted to the European Research Council for funding (ERC Starting Grant no 757501). A. C. is grateful to the French Ministry of National and Superior Education and Research (MENESR) for a PhD fellowship. F. F. M. gratefully acknowledges a Career Bridging Grant from TU Darmstadt. We are grateful to the CNRS (Centre National de la Recherche Scientifique) and the Technische Universität Darmstadt for providing access to facilities, specifically the Lichtenberg II high performance computer at TU Darmstadt on which all calculations for this work were performed.

Notes and references

Edge Article

1 A. D. Allen and C. V. Sen

- 1 A. D. Allen and C. V. Senoff, Nitrogenopentammineruthenium(II) complexes, *Chem. Commun.*, 1965, 621.
- 2 M. J. Chalkley, M. W. Drover and J. C. Peters, Catalytic N₂-to-NH₃ (or -N₂H₄) Conversion by Well-Defined Molecular Coordination Complexes, *Chem. Rev.*, 2020, **120**, 5582–5636.
- 3 Y. Roux, C. Duboc and M. Gennari, Molecular Catalysts for N₂ Reduction: State of the Art, Mechanism, and Challenges, *ChemPhysChem*, 2017, **18**, 2606–2617.
- 4 M. Pérez-Jiménez, H. Corona, F. de la Cruz-Martínez and J. Campos, Donor-Acceptor Activation of Carbon Dioxide, *Chem.-Eur. J.*, 2023, **29**, e202301428.
- 5 D. W. Stephan and G. Erker, Frustrated Lewis pair chemistry of carbon, nitrogen and sulfur oxides, *Chem. Sci.*, 2014, 5, 2625–2641.
- 6 A. E. Ashley and D. O'Hare, FLP-Mediated Activations and Reductions of CO₂ and CO, *Top. Curr. Chem.*, 2013, **334**, 191–217.
- 7 R. M. Bullock and G. M. Chambers, Frustration across the periodic table: heterolytic cleavage of dihydrogen by metal complexes, *Philos. Trans. R. Soc.*, *A*, 2017, 375, 20170002.
- 8 D. W. Stephan, Diverse Uses of the Reaction of Frustrated Lewis Pair (FLP) with Hydrogen, *J. Am. Chem. Soc.*, 2021, 143, 20002–20014.
- 9 M. A. Stevens and A. L. Colebatch, Cooperative approaches in catalytic hydrogenation and dehydrogenation, *Chem. Soc. Rev.*, 2022, **51**, 1881–1898.
- 10 J. C. Slootweg and A. R. Jupp, *Frustrated Lewis Pairs*, Springer Nature 2020
- 11 F.-G. Fontaine and D. W. Stephan, On the concept of frustrated Lewis pairs, *Philos. Trans. R. Soc.*, *A*, 2017, 375, 20170004.
- 12 D. W. Stephan, The broadening reach of frustrated Lewis pair chemistry, *Science*, 2016, 354, aaf7229.
- 13 D. W. Stephan, Frustrated Lewis Pairs: From Concept to Catalysis, *Acc. Chem. Res.*, 2015, **48**, 306–316.
- 14 D. W. Stephan and G. Erker, Frustrated Lewis Pair Chemistry: Development and Perspectives, *Angew. Chem., Int. Ed.*, 2015, 54, 6400-6441.
- 15 Frustrated Lewis Pairs II: Expanding the Scope, ed. G. Erker and D. W. Stephan, Springer Berlin Heidelberg, 2013.
- 16 Frustrated Lewis Pairs I: Uncovering and Understanding, ed. G. Erker and D. W. Stephan, Springer Berlin Heidelberg, 2013.
- 17 D. W. Stephan and G. Erker, Frustrated Lewis Pairs: Metalfree Hydrogen Activation and More, *Angew. Chem., Int. Ed.*, 2010, **49**, 46–76.
- 18 B. Chatterjee, W.-C. Chang, S. Jena and C. Werlé, Implementation of Cooperative Designs in Polarized Transition Metal Systems—Significance for Bond Activation and Catalysis, ACS Catal., 2020, 10, 14024–14055.
- 19 E. R. M. Habraken, A. R. Jupp, M. B. Brands, M. Nieger, A. W. Ehlers and J. C. Slootweg, Parallels between Metal-Ligand Cooperativity and Frustrated Lewis Pairs, *Eur. J. Inorg. Chem.*, 2019, 2019, 2436–2442.

- 20 P. C. Dos Santos, R. Y. Igarashi, H.-I. Lee, B. M. Hoffman, L. C. Seefeldt and D. R. Dean, Substrate Interactions with the Nitrogenase Active Site, *Acc. Chem. Res.*, 2005, 38, 208– 214.
- 21 T. Spatzal, K. A. Perez, O. Einsle, J. B. Howard and D. C. Rees, Ligand binding to the FeMo-cofactor: Structures of CObound and reactivated nitrogenase, *Science*, 2014, 345, 1620–1623.
- 22 S. M. Keable, J. Vertemara, O. A. Zadvornyy, B. J. Eilers, K. Danyal, A. J. Rasmussen, L. De Gioia, G. Zampella, L. C. Seefeldt and J. W. Peters, Structural characterization of the nitrogenase molybdenum-iron protein with the substrate acetylene trapped near the active site, *J. Inorg. Biochem.*, 2018, 180, 129–134.
- 23 D. Sippel, M. Rohde, J. Netzer, C. Trncik, J. Gies, K. Grunau, I. Djurdjevic, L. Decamps, S. L. A. Andrade and O. Einsle, A bound reaction intermediate sheds light on the mechanism of nitrogenase, *Science*, 2018, 359, 1484–1489.
- 24 W. Kang, C. C. Lee, A. J. Jasniewski, M. W. Ribbe and Y. Hu, Structural evidence for a dynamic metallocofactor during N₂ reduction by Mo-nitrogenase, *Science*, 2020, **368**, 1381–1385.
- 25 J. B. Geri, J. P. Shanahan and N. K. Szymczak, Testing the Push-Pull Hypothesis: Lewis Acid Augmented N₂ Activation at Iron, J. Am. Chem. Soc., 2017, 139, 5952–5956.
- 26 J. P. Shanahan and N. K. Szymczak, Hydrogen Bonding to a Dinitrogen Complex at Room Temperature: Impacts on N₂ Activation, *J. Am. Chem. Soc.*, 2019, **141**, 8550–8556.
- 27 J. J. Mortensen, B. Hammer and J. K. Nørskov, Alkali Promotion of N₂ Dissociation over Ru(0001), *Phys. Rev. Lett.*, 1998, **80**, 4333–4336.
- 28 S. Dahl, A. Logadottir, C. J. H. Jacobsen and J. K. Nørskov, Electronic factors in catalysis: the volcano curve and the effect of promotion in catalytic ammonia synthesis, *Appl. Catal.*, A, 2001, 222, 19–29.
- 29 G. P. Connor and P. L. Holland, Coordination chemistry insights into the role of alkali metal promoters in dinitrogen reduction, *Catal. Today*, 2017, **286**, 21–40.
- 30 Q. Wang, J. Guo and P. Chen, The impact of alkali and alkaline earth metals on green ammonia synthesis, *Chem*, 2021, 7, 3203–3220.
- 31 A. Coffinet, A. Simonneau and D. Specklin, in *Encyclopedia of Inorganic and Bioinorganic Chemistry*, ed. R. A. Scott, Wiley, 2nd edn, 2020, pp. 1–25.
- 32 A. J. Ruddy, D. M. C. Ould, P. D. Newman and R. L. Melen, Push and pull: the potential role of boron in N_2 activation, *Dalton Trans.*, 2018, 47, 10377–10381.
- 33 A. Simonneau and M. Etienne, Enhanced Activation of Coordinated Dinitrogen with p-Block Lewis Acids, *Chem. Eur. J.*, 2018, **24**, 12458–12463.
- 34 J. Chatt, J. R. Dilworth, R. L. Richards and J. R. Sanders, Chemical Evidence concerning the Function of Molybdenum in Nitrogenase, *Nature*, 1969, 224, 1201–1202.
- 35 J. Chatt, R. H. Crabtree and R. L. Richards, Dinitrogen- and carbonyl-complexes as bases towards trimethylaluminium, *J. Chem. Soc. Chem. Commun.*, 1972, 534.
- 36 J. Chatt, R. H. Crabtree, E. A. Jeffery and R. L. Richards, The basic strengths of some dinitrogen complexes of

molybdenum(0), tungsten(0), rhenium(I), and osmium(II), *J. Chem. Soc., Dalton Trans.*, 1973, 1167–1172.

Chemical Science

- 37 F. Studt, B. A. MacKay, S. A. Johnson, B. O. Patrick, M. D. Fryzuk and F. Tuczek, Lewis adducts of the side-on end-on dinitrogen-bridged complex [{(NPN)Ta}₂(μ-H)₂(μ-η1:η2-N₂)] with AlMe₃, GaMe₃, and B(C₆F₅)₃: Synthesis, structure, and spectroscopic properties, *Chem.-Eur. J.*, 2005, **11**, 604–618.
- 38 H. Broda, S. Hinrichsen, J. Krahmer, C. Nather and F. Tuczek, Molybdenum dinitrogen complexes supported by a silicon-centred tripod ligand and dppm or dmpm: tuning the activation of N₂, *Dalton Trans.*, 2014, 43, 2007–2012.
- 39 A. Simonneau, R. Turrel, L. Vendier and M. Etienne, Group 6 Transition-Metal/Boron Frustrated Lewis Pair Templates Activate N₂ and Allow its Facile Borylation and Silylation, *Angew. Chem., Int. Ed.*, 2017, **56**, 12268–12272.
- 40 D. Specklin, M.-C. Boegli, A. Coffinet, L. Escomel, L. Vendier, M. Grellier and A. Simonneau, An orbitally adapted pushpull template for N₂ activation and reduction to diazenediide, *Chem. Sci.*, 2023, 14, 14262–14270.
- 41 A. D. Piascik, P. J. Hill, A. D. Crawford, L. R. Doyle, J. C. Green and A. E. Ashley, Cationic silyldiazenido complexes of the $Fe(diphosphine)_2(N_2)$ platform: structural and electronic models for an elusive first intermediate in N_2 fixation, *Chem. Commun.*, 2017, 53, 7657–7660.
- 42 L. G. Pap, A. Couldridge, N. Arulsamy and E. Hulley, Electrostatic polarization of nonpolar substrates: a study of interactions between simple cations and Mo-bound N₂, *Dalton Trans.*, 2019, **48**, 11004–11017.
- 43 D. Specklin, A. Coffinet, L. Vendier, I. del Rosal, C. Dinoi and A. Simonneau, Synthesis, Characterization, and Comparative Theoretical Investigation of Dinitrogen-Bridged Group 6-Gold Heterobimetallic Complexes, *Inorg. Chem.*, 2021, 60, 5545–5562.
- 44 C. Tang, Q. Liang, A. R. Jupp, T. C. Johnstone, R. C. Neu, D. Song, S. Grimme and D. W. Stephan, 1,1-Hydroboration and a Borane Adduct of Diphenyldiazomethane: A Potential Prelude to FLP-N₂ Chemistry, *Angew. Chem., Int. Ed.*, 2017, 56, 16588–16592.
- 45 F. F. Martins and V. Krewald, Cooperative Dinitrogen Activation: Identifying the Push–Pull Effects of Transition Metals and Lewis Acids in Molecular Orbital Diagrams, *Eur. J. Inorg. Chem.*, 2023, 26, e202300268.
- 46 L. Greb, Lewis Superacids: Classifications, Candidates, and Applications, *Chem.–Eur. J.*, 2018, **24**, 17881–17896.
- 47 J. L. W. Pohlmann and F. E. Brinckmann, Preparation and Characterization of Group III A Derivatives, *Z. Naturforsch. B*, 1965, **20**, 5–11.
- 48 T. Belgardt, J. Storre, H. W. Roesky, M. Noltemeyer and H.-G. Schmidt, Tris(pentafluorophenyl)alane: A Novel Aluminum Organyl, *Inorg. Chem.*, 1995, 34, 3821–3822.
- 49 G. S. Hair, A. H. Cowley, R. A. Jones, B. G. McBurnett and A. Voigt, Arene Complexes of Al(C6F5)3. Relationship to a Déjà Vu Silylium Ion, *J. Am. Chem. Soc.*, 1999, **121**, 4922–4923.

- 50 J. Klosin, G. R. Roof, E. Y.-X. Chen and K. A. Abboud, Ligand Exchange and Alkyl Abstraction Involving (Perfluoroaryl) boranes and -alanes with Aluminum and Gallium Alkyls, Organometallics, 2000, 19, 4684–4686.
- 51 S. Feng, G. R. Roof and E. Y.-X. Chen, Tantalum(V)-Based Metallocene, Half-Metallocene, and Non-Metallocene Complexes as Ethylene–1-Octene Copolymerization and Methyl Methacrylate Polymerization Catalysts, *Organometallics*, 2002, 21, 832–839.
- 52 N. G. Stahl, M. R. Salata and T. J. Marks, $B(C_6F_5)_3$ vs $Al(C_6F_5)_3$ -Derived Metallocenium Ion Pairs. Structural, Thermochemical, and Structural Dynamic Divergences, *J. Am. Chem. Soc.*, 2005, **127**, 10898–10909.
- 53 J. Chen and E. Y.-X. Chen, Unsolvated $Al(C_6F_5)_3$: structural features and electronic interaction with ferrocene, *Dalton Trans.*, 2016, 45, 6105–6110.
- 54 D. M. C. Ould, J. L. Carden, R. Page and R. L. Melen, Synthesis and Reactivity of Fluorinated Triaryl Aluminum Complexes, *Inorg. Chem.*, 2020, 59, 14891–14898.
- 55 I. V. Kazakov, A. S. Lisovenko, N. A. Shcherbina, I. V. Kornyakov, N. Y. Gugin, Y. V. Kondrat'ev, A. M. Chernysheva, A. S. Zavgorodnii and A. Y. Timoshkin, Structural and Energetic Features of Group 13 Element Trispentafluorophenyl Complexes with Diethyl Ether, Eur. J. Inorg. Chem., 2020, 2020, 4442–4449.
- 56 A. Y. Timoshkin, The Field of Main Group Lewis Acids and Lewis Superacids: Important Basics and Recent Developments, *Chem.–Eur. J.*, 2024, **30**, e202302457.
- 57 L. Pauling, Atomic Radii and Interatomic Distances in Metals, *J. Am. Chem. Soc.*, 1947, **69**, 542–553.
- 58 W. E. Piers and T. Chivers, Pentafluorophenylboranes: from obscurity to applications, *Chem. Soc. Rev.*, 1997, **26**, 345.
- 59 J. R. Lawson and R. L. Melen, Tris(pentafluorophenyl)borane and Beyond: Modern Advances in Borylation Chemistry, *Inorg. Chem.*, 2017, 56, 8627–8643.
- 60 J. Chen and E. Y. -X. Chen, Elusive Silane–Alane Complex [Si H····Al]: Isolation, Characterization, and Multifaceted Frustrated Lewis Pair Type Catalysis, *Angew. Chem., Int. Ed.*, 2015, 54, 6842–6846.
- 61 K. O. Christe, D. A. Dixon, D. McLemore, W. W. Wilson, J. A. Sheehy and J. A. Boatz, On a quantitative scale for Lewis acidity and recent progress in polynitrogen chemistry, J. Fluorine Chem., 2000, 101, 151–153.
- 62 J. C. Haartz and D. H. McDaniel, Fluoride ion affinity of some Lewis acids, *J. Am. Chem. Soc.*, 1973, **95**, 8562–8565.
- 63 E. Y.-X. Chen, W. J. Kruper, G. Roof and D. R. Wilson, Double Activation of Constrained Geometry and *ansa*-Metallocene Group 4 Metal Dialkyls: Synthesis, Structure, and Olefin Polymerization Study of Mono- and Dicationic Aluminate Complexes, *J. Am. Chem. Soc.*, 2001, 123, 745–746.
- 64 A. Y. Timoshkin and G. Frenking, Gas-Phase Lewis Acidity of Perfluoroaryl Derivatives of Group 13 Elements, *Organometallics*, 2008, 27, 371–380.
- 65 J. F. Kögel, D. A. Sorokin, A. Khvorost, M. Scott, K. Harms, D. Himmel, I. Krossing and J. Sundermeyer, The Lewis superacid $Al[N(C_6F_5)_2]_3$ and its higher homolog Ga $[N(C_6F_5)_2]_3$ structural features, theoretical investigation

Edge Article

and reactions of a metal amide with higher fluoride ion affinity than SbF₅, Chem. Sci., 2017, **9**, 245–253.

- 66 T. A. George and M. E. Noble, A direct one-step preparation of bis(dinitrogen) complexes of molybdenum(0) from molybdenum(V) chloride, *Inorg. Chem.*, 1978, 17, 1678–1679.
- 67 J. R. Dilworth, R. L. Richards, G. J.-J. Chen and J. W. Mcdonald, in *Inorganic Syntheses*, John Wiley & Sons, Ltd, 1990, pp. 33–43.
- 68 R. Poli and H. D. Mui, True nature of trihalotris(tetrahydrofuran)molybdenum(III), MoX₃(THF)₃ (X = Cl, Br, I). A paramagnetic proton NMR study, *J. Am. Chem. Soc.*, 1990, **112**, 2446–2448.
- 69 F. Stoffelbach, D. Saurenz and R. Poli, Improved Preparations of Molybdenum Coordination Compounds from Tetrachlorobis(diethyl ether)molybdenum(IV), Eur. J. Inorg. Chem., 2001, 2699–2703.
- 70 A. C. Filippou, G. Schnakenburg, A. I. Philippopoulos and N. Weidemann, Ge₂ trapped by triple bonds between two metal centers: the germylidyne complexes trans,trans-[Cl(depe)₂M≡Ge—Ge≡M(depe)₂Cl] (M=Mo, W) and bonding analyses of the M≡Ge—Ge≡M chain, *Angew. Chem., Int. Ed.*, 2005, 44, 5979–5985.
- 71 E. M. Zolnhofer, A. A. Opalade, T. A. Jackson, F. W. Heinemann, K. Meyer, J. Krzystek, A. Ozarowski and J. Telser, Electronic Structure and Magnetic Properties of a Low-Spin Cr^{II} Complex: trans-[CrCl₂(dmpe)₂] (dmpe = 1,2-Bis(dimethylphosphino)ethane), Inorg. Chem., 2021, 60, 17865–17877.
- 72 G. S. Girolami, G. Wilkinson, A. M. R. Galas, M. Thornton-Pett and M. B. Hursthouse, Synthesis and properties of the divalent 1,2-bis(dimethylphosphino)ethane (dmpe) complexes MCl₂(dmpe)₂ and MMe₂(dmpe)₂ (M = Ti, V, Cr, Mn, or Fe). X-Ray crystal structures of MCl₂(dmpe)₂ (M = Ti, V, or Cr), MnBr₂(dmpe)₂, TiMe_{1.3}Cl_{0.7}(dmpe)₂, and CrMe₂(dmpe)₂, J. Chem. Soc., Dalton Trans., 1985, 1339.
- 73 A. J. Kendall, S. I. Johnson, R. M. Bullock and M. T. Mock, Catalytic Silylation of N₂ and Synthesis of NH₃ and N₂H₄ by Net Hydrogen Atom Transfer Reactions Using a Chromium P₄ Macrocycle, J. Am. Chem. Soc., 2018, 140, 2528–2536.
- 74 J. E. Salt, G. S. Girolami, G. Wilkinson, M. Motevalli, M. Thornton-Pett and M. B. Hursthouse, Synthesis and characterisation of 1,2-bis(dimethylphosphino)ethane (dmpe) complexes of chromium-(0) and -(IV): X-ray crystal structures of trans-Cr(N₂)₂(dmpe)₂, cis-Cr(CO)₂(dmpe)₂, Cr(C₂Ph₂)₂(dmpe), and CrH₄(dmpe)₂, *J. Chem. Soc., Dalton Trans.*, 1985, 685.
- 75 L. A. Berben and S. A. Kozimor, Dinitrogen and Acetylide Complexes of Low-Valent Chromium, *Inorg. Chem.*, 2008, 47, 4639–4647.
- 76 J. He, Y. Zhang, L. Falivene, L. Caporaso, L. Cavallo and E. Y.-X. Chen, Chain Propagation and Termination Mechanisms for Polymerization of Conjugated Polar Alkenes by [Al]-Based Frustrated Lewis Pairs, *Macromolecules*, 2014, 47, 7765–7774.
- 77 L. L. Cao, J. Zhou, Z. Qu and D. W. Stephan, Single Electron Transfer to Diazomethane–Borane Adducts Prompts C–H

- Bond Activations, Angew. Chem., Int. Ed., 2019, 58, 18487-18491.
- 78 T. Asada, Y. Hoshimoto and S. Ogoshi, Rotation-Triggered Transmetalation on a Heterobimetallic Cu/Al *N*-Phosphine-Oxide-Substituted Imidazolylidene Complex, *J. Am. Chem. Soc.*, 2020, **142**, 9772–9784.
- 79 Z. Yu, M. J. Heeg and C. H. Winter, A bridging ethyl complex of aluminium, *Chem. Commun.*, 2001, 353–354.
- 80 W. Uhl and F. Hannemann, A methylene bridged dialuminium compound as a chelating Lewis acid—complexation of azide and acetate anions by R₂Al-CH₂-AlR₂ [R=CH(SiMe₃)₂], *J. Organomet. Chem.*, 1999, 579, 18-23.
- 81 J. Liu, T.-L. Lam, M.-K. Sit, Q. Wan, C. Yang, G. Cheng and C.-M. Che, Pure blue phosphorescent platinum(ii) emitters supported by NHC-based pincer type ligands with unitary emission quantum yields, *J. Mater. Chem. C*, 2022, **10**, 10271–10283.
- 82 T. Voss, T. Mahdi, E. Otten, R. Fröhlich, G. Kehr, D. W. Stephan and G. Erker, Frustrated Lewis Pair Behavior of Intermolecular Amine/B(C₆F₅)₃ Pairs, Organometallics, 2012, 31, 2367–2378.
- 83 K. Bläsing, J. Bresien, R. Labbow, D. Michalik, A. Schulz, M. Thomas and A. Villinger, Borane Adducts of Hydrazoic Acid and Organic Azides: Intermediates for the Formation of Aminoboranes, *Angew. Chem., Int. Ed.*, 2019, 58, 6540– 6544.
- 84 W. Uhl, F. Hannemann, W. Saak and R. Wartchow, Diazomethane Derivatives Bearing Dialkylaluminium or DialkylgalliumSubstituents The Isomeric Diazomethane and Nitrile Imine Structures Realized by the Different Coordination Behavior of Aluminium and Gallium, *Eur. J. Inorg. Chem.*, 1999, 1999, 771–776.
- 85 B. L. Nordwig, D. J. Ohlsen, K. D. Beyer, A. S. Wruck and J. G. Brummer, The Effect of the Diphosphine Basicity on the Excited-State Properties of *trans*-(N₂)₂W(R₂PCH₂CH₂PR₂)₂: Identification of Near-Degenerate, Luminescent ³MLCT and ³LF Terms, *Inorg. Chem.*, 2006, 45, 858–867.
- 86 F. Maschietto, M. Campetella, J. Sanz García, C. Adamo and I. Ciofini, Chasing unphysical TD-DFT excited states in transition metal complexes with a simple diagnostic tool, *J. Chem. Phys.*, 2021, 154, 204102.
- 87 Y. Sun, S. N. Collins, L. E. Joyce and C. Turro, Unusual Photophysical Properties of a Ruthenium(II) Complex Related to [Ru(bpy)₂ (dppz)]²⁺, *Inorg. Chem.*, 2010, 49, 4257–4262.
- 88 T. Knoell, J. Polanco, S. N. MacMillan, J. A. Bertke, C. Foroutan-Nejad, K. M. Lancaster and A. Gus Bakhoda, Alkaline earth metal-assisted dinitrogen activation at nickel, *Dalton Trans.*, 2024, 53, 4689–4697.
- 89 X. Wang, Y. Wang, Y. Wu, G.-X. Wang, J. Wei and Z. Xi, Syntheses and Characterizations of Hetero-Bimetallic Chromium-Dinitrogen Transition-Metal Complexes, *Inorg. Chem.*, 2023, **62**, 18641–18648.
- 90 B. A. Suslick and T. D. Tilley, Mechanistic Interrogation of Alkyne Hydroarylations Catalyzed by Highly Reduced,

Open Access Article. Published on 17 2024. Downloaded on 04/11/2025 05:58:21

Chemical Science

- Single-Component Cobalt Complexes, *J. Am. Chem. Soc.*, 2020, **142**, 11203–11218.
- 91 S. L. Apps, P. W. Miller and N. J. Long, Cobalt(-i) triphos dinitrogen complexes: activation and silyl-functionalisation of N₂, *Chem. Commun.*, 2019, 55, 6579–6582.
- 92 T. D. Lohrey, R. G. Bergman and J. Arnold, Controlling dinitrogen functionalization at rhenium through alkali metal ion pairing, *Dalton Trans.*, 2019, 48, 17936–17944.
- 93 T. R. Dugan, K. C. MacLeod, W. W. Brennessel and P. L. Holland, Cobalt–Magnesium and Iron–Magnesium Complexes with Weakened Dinitrogen Bridges, Eur. J. Inorg. Chem., 2013, 2013, 3891–3897.
- 94 T. A. Betley and J. C. Peters, Dinitrogen Chemistry from Trigonally Coordinated Iron and Cobalt Platforms, *J. Am. Chem. Soc.*, 2003, **125**, 10782–10783.
- 95 G. E. Greco and R. R. Schrock, Synthesis, Structure, and Electrochemical Studies of Molybdenum and Tungsten Dinitrogen, Diazenido, and Hydrazido Complexes That Contain Aryl-Substituted Triamidoamine Ligands, *Inorg. Chem.*, 2001, 40, 3861–3878.

- 96 M. B. O'Donoghue, W. M. Davis, R. R. Schrock and W. M. Reiff, Heterobimetallic Dinitrogen Complexes That Contain the {[N₃N]Mo-NN}⁻ Ligand, *Inorg. Chem.*, 1999, **38**, 243-252.
- 97 M. B. O'Donoghue, W. M. Davis and R. R. Schrock, Derivatization of Dinitrogen by Molybdenum in Triamidoamine Complexes, *Inorg. Chem.*, 1998, 37, 5149–5158.
- 98 H. F. Klein, H. Koenig, S. Koppert, K. Ellrich and J. Riede, Cobalt diazenides of Main Group 1-3 metals: X-ray structure of a Grignard compound containing (dinitrogen)(trimethylphosphine)cobaltate anions, *Organometallics*, 1987, 6, 1341–1345.
- 99 N. Jori, J. J. Moreno, R. A. K. Shivaraam, T. Rajeshkumar, R. Scopelliti, L. Maron, J. Campos and M. Mazzanti, Iron promoted end-on dinitrogen-bridging in heterobimetallic complexes of uranium and lanthanides, *Chem. Sci.*, 2024, 15, 6842–6852.